Internal equilibration of a nucleus with metastable states: ^{26}Al as an example

Sanjib S. Gupta and Bradley S. Meyer

Department of Physics and Astronomy, Clemson University, Clemson, South Carolina 29634-0978

In many isotopes important to nucleosynthesis theory there exists a low-lying metastable state whose deexcitation to the ground state is strongly inhibited by a large angular momentum difference. In a stellar plasma, the equilibration of the ground and metastable states of such nuclei proceeds primarily via indirect transitions that involve upper-lying levels. We present a mathematical technique to follow these multistep transitions. Under the crucial assumption that the abundances of the upper-lying levels are in a steady-state abundance distribution, our method abstracts away all the higher-lying excited states allowing the isotope in question to be represented as a two-state system with transitions between these two states. The two states are properly not the ground and metastable states themselves but rather two ensembles of states, one tied to the ground state and one tied to the metastable state. We show how to compute effective rates into and out of these ensembles and between them, as well as how to identify the dominant pathways. This allows such nuclei to be treated in a simple, straightforward, and accurate fashion in nucleosynthesis networks. The specific example of ^{26}Al, including its effective beta-decay lifetime, is considered in detail.

I. INTRODUCTION

The rates for key nuclear reactions are crucial inputs for models of stellar evolution and nucleosynthesis. The lack of an accurate value for the rate of one or more nuclear reactions frequently limits the conclusions that may be drawn from an astrophysical model. As a salient example, the uncertainties that currently exist in the experimentally available $^{12}C(\alpha, \gamma)^{16}O$ reaction rate constrain the accuracy of stellar models beyond the phase of helium burning (e.g., see Ref. [1]). Clearly, continued progress in stellar modeling and nucleosynthesis will require ongoing efforts in nuclear physics laboratories.

While nuclear physics experiments underpin the success of astrophysics models by providing essential input, it has not always been true that Earth-bound laboratories provide precisely the information required by the models. For example, only recently have experimentalists begun measuring reaction rates at the low energies relevant to the conditions at the center of the sun [2]. A similar problem that will prove even more challenging is the issue of the excited states in target nuclei.

Laboratory measurements of nuclear reaction rates are made on target nuclei in their ground states. In a stellar plasma, however, the target nuclei are distributed among their excited states. This is a well-known problem, but a proper accounting of this in stellar models has not proven easy. Ultimately one would wish for direct experiments, but this will be extremely difficult in Earth-bound laboratories. For now one must seek to make the laboratory results on ground-state nuclei more appropriate for stellar models. The simplest approach is that of an "equal strength approximation" [3], in which the rate for some reaction on a nucleus in an excited state is assumed to be equal to that when the nucleus is in its ground state. More recently, there have been efforts to account for the excited states more accurately by using experimental nuclear level data or by using Hauser-Feshbach calculations and the assumption of a thermal population of excited states to give corrections to the ground-state rates (e.g., see Ref. [4]).

Generally, the internal equilibration of a nucleus occurs more rapidly than the competing processes of production or destruction of that nucleus. In such a case, an equilibrium population of excited states is a reasonable approximation. In certain isotopes, however, a low-lying isomeric state is only directly connected to the ground state by a transition of high multipolarity. This strongly inhibits internal equilibration of the nucleus, and consequently the distribution of such nuclei among their excited states cannot be treated by Boltzmann statistics. In such a case, equilibration of the isomer and the ground state occurs only indirectly via upper-lying levels, and it is frequently necessary to treat the two states, or, more properly, two ensembles of states, one tied to the ground state and one tied to the long-lived isomer, as separate species in the nuclear reaction network.

Fortunately, the number of such isotopes is small. However, among their number is ^{26}Al. The 5^+ ground state of ^{26}Al has a million-year lifetime against β^+ decay, which makes it of great interest for gamma-ray astronomy (e.g., see Ref. [5]), cosmochemistry (e.g., see Ref. [6]), and the study of presolar grains (e.g., see Ref. [7]). The 0^+ first excited state at 0.228 MeV, on the other hand, lives for only 9.2 s. This complicates the effective ^{26}Al decay rate in a stellar plasma. The effective decay rate would be easy to compute, if the 5^+ and 0^+ states communicated efficiently, for then one could assume they existed in an equilibrium thermal distribution. The large difference in spin between the two states inhibits their direct communication, however, and one is usually forced to treat them as separate nuclear species in reaction networks. This is not too difficult in practice—one simply needs to follow the reactions that separately feed and destroy these two species. What is lacking, however, is a simple-to-use and accurate rate for the transition *between* the two species. Such a transition becomes important near 0.4 $\times 10^9$ K ($T_9 = 0.4$) at which temperature internal equilibration of ^{26}Al competes with beta decay from the metastable

64 025805-1

state. Our goal in this paper is to calculate the rate for this transition and to show how to use it in a reaction network. Other nuclei where such long-lived isomeric states play a crucial role in nucleosynthesis theory include ^{85}Kr, ^{113}Cd, ^{115}Cd, and ^{115}In and ^{180}Ta. We will present detailed treatments of these nuclei in subsequent papers.

Ward and Fowler [8] have described and investigated this problem in some detail. More recently, Coc, Porquet, and Nowacki have computed the effective beta-decay lifetime of ^{26}Al in a stellar plasma [9] using new shell-model calculations of the rates of certain internal transitions not known from experiment. In both of the above papers, the authors presented results of internal equilibration from numerical calculations. We revisit this problem in what we believe is a more straightforward manner. The key to our approach is the assumption that the nuclear levels in ^{26}Al lying higher in energy than the ground and metastable states are in a steady state. With this largely accurate assumption of a steady state, we then exploit the combinatorial nature of the problem to compute the effective rate of equilibration of the ground and metastable states by enumerating all possible pathways via upper-lying levels. Apart from the intellectual appeal of the resulting interpretation, this method allows for a direct evaluation of the importance of any nuclear level or transition to the overall equilibration rate. Moreover, the treatment is quite general and is applicable to any similar nucleus, if not more generally to the kinetics of analogous atomic and molecular systems exhibiting important nonequilibrium effects in a plasma.

Our technique also permits direct calculation of the degree of connection of an upper-lying level to the ground or metastable state. This allows us (under the good assumption of a steady state among the upper-lying levels) to separate the nuclear levels in ^{26}Al into two ensembles of states with each level participating in *both* ensembles. In this way we are then able to compute effective rates for transitions from either ensemble to other nuclear species or vice versa and for transitions between the two ensembles of states. These two ensembles, then, are properly the two separate species one evolves in the nuclear reaction network, and we have successfully transformed the problem for the multilevel nucleus to that of an equivalent two-level system.

The outline of the paper is as follows. Section II treats the steady-state approximation and computes the effective transition rate between the isomer and ground state. Section III provides a combinatorial interpretation of the effective rate. Section IV applies the effective rate to the specific case of ^{26}Al, while Sec. V explores the kinetics of internal equilibration in further detail. Section VI discusses our approach to treating a nucleus with a long-lived isomeric state as two separate species in a reaction network, and Sec. VII presents a brief summary.

II. THE STEADY-STATE APPROXIMATION

A simple example motivates our basic technique for treating metastable-state nuclei, such as ^{26}Al. Consider the abundance Y of a single nuclear species with a constant rate of production P and a rate of destruction λ per nucleus. The abundance is governed by

$$\frac{dY}{dt} = -\lambda Y + P, \tag{2.1}$$

which has the solution

$$Y(t) = Y(0)e^{-\lambda t} + \left(\frac{P}{\lambda}\right)(1 - e^{-\lambda t}), \tag{2.2}$$

where $Y(0)$ is the initial abundance. The long-time behavior $(t \to \infty)$ is such that $(dY/dt) \to 0$. Equation (2.2) leads to the following conclusions.

The timescale $\sim (1/\lambda)$ for achieving a steady state is determined by the destruction rate λ;

(i) The steady-state abundance is given by (P/λ), i.e., by the ratio (production rate/destruction rate per nucleus).

(ii) Consider next the situation in a three-level system with level indices arranged in order of increasing energies (this convention will be followed throughout), with the added provision that level 2 may not communicate directly with the ground state (level 1). This may occur, for example, if the spin difference between the two lower levels is very high, in which case the levels communicate only slowly via a very high order multipole.

The relevant equations governing the evolution of the abundances in the three-level system are then

$$\frac{dY_1}{dt} = -\Lambda_1 Y_1 + \lambda_{31} Y_3, \tag{2.3}$$

$$\frac{dY_2}{dt} = -\Lambda_2 Y_2 + \lambda_{32} Y_3, \tag{2.4}$$

$$\frac{dY_3}{dt} = -\Lambda_3 Y_3 + \lambda_{13} Y_1 + \lambda_{23} Y_2, \tag{2.5}$$

where λ_{ij} represents the rate for the transitions *from* level *i to* level *j* and

$$\Lambda_k = \sum_{j \neq k} \lambda_{kj} \tag{2.6}$$

represents the total rate for the destruction of level *k*.

Λ_1 and Λ_2 are exclusively determined from upward transitions; therefore, at sufficiently low temperatures, they will typically be many orders of magnitude smaller than Λ_3 (which involves downward transitions). We thus postulate that level 3 reaches a steady state on a short timescale compared to the timescale on which the abundances of levels 1 and 2 change; hence, we may set $(dY_3/dt) = 0$ in Eq. (2.5). Note that this assumption corresponds to treating transitions out of level 3 as instantaneous. Such an approximation enables us to immediately solve for Y_3 in terms of Y_1 and Y_2:

$$Y_3(t) = \left\{ \frac{\lambda_{13} Y_1 + \lambda_{23} Y_2}{\Lambda_3} \right\}. \tag{2.7}$$

Substituting Eq. (2.7) into Eqs. (2.3) and (2.4), we obtain a two-species network

$$\frac{dY_1}{dt} = AY_1 + BY_2, \tag{2.8}$$

$$\frac{dY_2}{dt} = CY_1 + DY_2, \tag{2.9}$$

where the coefficients may be obtained by inspection,

$$A = \left\{ -\lambda_{13} + \left(\frac{\lambda_{13}\lambda_{31}}{\Lambda_3} \right) \right\} = -\lambda_{13}(1 - f_{31}), \tag{2.10}$$

$$B = \left(\frac{\lambda_{23}\lambda_{31}}{\Lambda_3} \right) = \lambda_{23}f_{31}, \tag{2.11}$$

$$C = \left(\frac{\lambda_{13}\lambda_{32}}{\Lambda_3} \right) = \lambda_{13}f_{32}, \tag{2.12}$$

$$D = \left\{ -\lambda_{23} + \left(\frac{\lambda_{23}\lambda_{32}}{\Lambda_3} \right) \right\} = -\lambda_{23}(1 - f_{32}), \tag{2.13}$$

where f_{ij} denotes the branching ratio or the probability that a transition out of level i will be to level j,

$$f_{ij} = \frac{\lambda_{ij}}{\Lambda_i}. \tag{2.14}$$

A, B, C, and D are not independent quantities since $f_{31} + f_{32} = 1$ implies that $A = -C$ and $D = -B$. Thus, we obtain two effective rates for our two-level system,

$$\frac{dY_1}{dt} = -\lambda_{12}^{eff}Y_1 + \lambda_{21}^{eff}Y_2,$$

$$\frac{dY_2}{dt} = \lambda_{12}^{eff}Y_1 - \lambda_{21}^{eff}Y_2, \tag{2.15}$$

where

$$\lambda_{12}^{eff} = \lambda_{13}f_{32}, \tag{2.16}$$

$$\lambda_{21}^{eff} = \lambda_{23}f_{31}. \tag{2.17}$$

Usually it is only the downward spontaneous decay rates that are known from experiment or theoretical shell-model calculations. Nevertheless, from this information, it is possible to use the Einstein relations to compute the induced upward and downward transition rates in a high-temperature plasma. In this way, the effective rates λ_{12}^{eff} and λ_{21}^{eff} can be completely specified. In this paper we neglect transitions induced by collisions with other ions in the plasma. In general, these contribute to the overall internal transition rates only at the highest temperatures and densities [8,15]. Nevertheless, their inclusion would be straightforward in our formalism.

We now generalize to an n-level system with a ground state (level 1) and a low-lying metastable state (level 2) that do not communicate via a direct transition. Since the total destruction rates out of levels 1 and 2 are calculated exclusively from upward transitions to higher-lying states we have

$$\Lambda_k \gg \Lambda_1 \quad \text{and} \quad \Lambda_k \gg \Lambda_2 \tag{2.18}$$

for levels $k > 2$. Hence, we may assume the higher-lying levels attain steady states on short timescales compared to $(1/\Lambda_1)$ or $(1/\Lambda_2)$, i.e., $(dY_k/dt) = 0$ for levels $k > 2$. Note however that dY_1/dt and dY_2/dt are *not* equal to zero because their timescales to reach a steady state are much longer. The abundances in the full nuclear reaction network are governed by n equations of the form

$$\frac{dY_k}{dt} = \lambda_{1k}Y_1 + \lambda_{2k}Y_2 + \lambda_{3k}Y_3 + \cdots + \lambda_{k-1,k}Y_{k-1} - \Lambda_k Y_k$$

$$+ \lambda_{k+1,k}Y_{k+1} + \cdots + \lambda_{nk}Y_n, \tag{2.19}$$

where $1 \leq k \leq n$. For levels $k > 2$ we may set the left-hand side of Eq. (2.19) to zero and obtain $(n-2)$ equations of the form

$$-\lambda_{3k}Y_3^{SS} - \cdots - \lambda_{k-1,k}Y_{k-1}^{SS} + \Lambda_k Y_k^{SS} - \lambda_{k+1,k}Y_{k+1}^{SS} - \cdots$$

$$- \lambda_{nk}Y_n^{SS} = \lambda_{1k}Y_1 + \lambda_{2k}Y_2, \tag{2.20}$$

where now $3 \leq k \leq n$ and Y_k^{SS} denotes the steady-state abundance of level k. This system of linear equations may be immediately recast in matrix form as

$$
\begin{pmatrix}
\Lambda_3 & -\lambda_{43} & -\lambda_{53} & -\cdots & -\cdots & -\cdots & -\lambda_{n3} \\
-\lambda_{34} & \Lambda_4 & -\lambda_{54} & -\cdots & -\cdots & -\cdots & -\lambda_{n4} \\
\vdots & \vdots & \vdots & \vdots & \vdots & \vdots & \vdots \\
-\lambda_{3n} & -\lambda_{4n} & -\lambda_{5n} & -\cdots & -\cdots & -\cdots & \Lambda_n
\end{pmatrix}
$$

$$
\times
\begin{pmatrix}
Y_3^{SS} \\
Y_4^{SS} \\
\vdots \\
Y_n^{SS}
\end{pmatrix}
=
\begin{pmatrix}
\lambda_{13}Y_1 + \lambda_{23}Y_2 \\
\lambda_{14}Y_1 + \lambda_{24}Y_2 \\
\vdots \\
\lambda_{1n}Y_1 + \lambda_{2n}Y_2
\end{pmatrix}, \tag{2.21}
$$

which enables a solution of the steady-state abundances by first defining the following algebraic entities:

(i) The diagonal destruction matrix, with $\Lambda_{ij} = \delta_{ij}\Lambda_i$ (for $3 \leq i,j \leq n$). That is, Λ has the destruction rates of levels $3 - n$ on its diagonal and zero everywhere else. The inverse diagonal destruction matrix Λ^{-1} then has the elements $(\Lambda^{-1})_{ij} = (\delta_{ij}/\Lambda_i)$ (for $3 \leq i,j \leq n$);

(ii) The identity matrix of order $(n-2)$ denoted by I;

(iii) The "transfer matrix" F given by $F_{ij} = f_{ij}$ (for $3 \leq i,j \leq n$). This is the transition probability matrix of the subsystem formed by excluding the ground and the metastable states. Its transpose will be denoted by $F^\mathbf{T}$;

(iv) The steady-state abundance vector

$$
Y^{SS} =
\begin{pmatrix}
Y_3^{SS} \\
\vdots \\
Y_n^{SS}
\end{pmatrix};
$$

(v) The "production vectors"

$$\lambda_q^{out} = \begin{pmatrix} \lambda_{q3} \\ \vdots \\ \lambda_{qn} \end{pmatrix} = \Lambda_q \begin{pmatrix} f_{q3} \\ \vdots \\ f_{qn} \end{pmatrix} \equiv \Lambda_q f_q^{out}$$

comprised of the rates from the ground ($q=1$) and meta-stable states ($q=2$), respectively, "out" to all the upper-lying levels; and

(vi) The "total production vector"

$$P = \lambda_1^{out} Y_1 + \lambda_2^{out} Y_2 = \begin{pmatrix} \lambda_{13} Y_1 + \lambda_{23} Y_2 \\ \vdots \\ \lambda_{1n} Y_1 + \lambda_{2n} Y_2 \end{pmatrix},$$

which is the right-hand side of Eq. (2.21).

With these definitions, Eq. (2.21) becomes

$$(I - F^T) \Lambda Y^{SS} = P, \qquad (2.22)$$

which may be immediately solved for the steady-state abundances,

$$Y^{SS} = \Lambda^{-1} (I - F^T)^{-1} P. \qquad (2.23)$$

Now, F^T is merely the transpose of the transition probability matrix with all transitions to and from levels 1 and 2 removed. This classifies F^T as a *principal submatrix* of a *stochastic* matrix. The parent stochastic matrix is *irreducible* since no proper subset of levels can form a closed system. We can then use a theorem of Frobenius for a nonnegative irreducible matrix that declares its maximal eigenvalue modulus (*spectral radius*) to be strictly greater than that of any principal submatrix [10]. This implies that the spectral radius of F^T is strictly less than unity, since all stochastic matrices have a unit spectral radius [11]. Then the Lagrange-Sylvester theorem for matrices [11] implies that $(I - F^T)$ is nonsingular and that we may expand its inverse in a matrix series,

$$(I - F^T)^{-1} = I + F^T + (F^T)^2 + (F^T)^3 + \cdots = F_\infty^T. \qquad (2.24)$$

Let us denote the Nth partial sum of this series by F_N^T and note that

$$F_N^T = I + F^T + (F^T)^2 + \cdots + (F^T)^{N-1}$$
$$= I + F^T + (F^2)^T + \cdots + (F^{N-1})^T = (F_N)^T. \quad (2.25)$$

Substituting this result into Eq. (2.23), we obtain the compact approximation

$$Y^{SS} \approx Y_N^{SS} \equiv \Lambda^{-1} F_N^T P \qquad (2.26)$$

correct to order N in the maximum number of intermediate levels participating in the indirect transitions between levels 2 and 1.

To determine the effective transition rates between levels 1 and 2, we next define the vector f_q^{in} as

$$f_q^{in} \equiv \begin{pmatrix} f_{3q} \\ \vdots \\ f_{nq} \end{pmatrix}, \qquad (2.27)$$

where $q=1$ corresponds to the ground state and $q=2$ corresponds to the metastable state. With this definition, we may estimate λ_{21}^{eff} by rewriting Eq. (2.19) with $k=1$,

$$\frac{dY_1}{dt} = -\Lambda_1 Y_1 + \sum_{k>2} \lambda_{k1} Y_k^{SS}$$
$$= -\Lambda_1 Y_1 + (f_1^{in})^T \Lambda Y^{SS}$$
$$\approx -\Lambda_1 Y_1 + (f_1^{in})^T \Lambda (\Lambda^{-1} F_N^T P)$$
$$= -\Lambda_1 Y_1 + (f_1^{in})^T F_N^T (\Lambda_1 f_1^{out} Y_1 + \Lambda_2 f_2^{out} Y_2).$$
$$(2.28)$$

Comparing Eqs. (2.15) and (2.28), we immediately have

$$\lambda_{21}^{eff} \approx \lambda_{21,N}^{eff} = \Lambda_2 (f_1^{in})^T F_N^T f_2^{out} = \Lambda_2 [(f_2^{out})^T F_N f_1^{in}]. \qquad (2.29)$$

The second equation follows because λ_{21}^{eff} is a scalar quantity. By exactly similar reasoning, one may find

$$\lambda_{12}^{eff} \approx \lambda_{12,N}^{eff} = \Lambda_1 \{ (f_1^{out})^T F_N f_2^{in} \}. \qquad (2.30)$$

Our expressions for the effective rates between levels 1 and 2 are approximations to the exact solution since we consider F_N rather than F_∞. However, we may approximate the exact solution to arbitrary accuracy by choosing a suitably large value for N. The fractional error involved in the series truncation may be estimated using the easily computed matrix ∞ norm. For any $m \times m$ matrix F, the ∞ norm is merely the *maximum row sum*, which for a substochastic matrix F is guaranteed to be strictly less than unity:

$$\|F\| \equiv \|F\|_\infty = \max_i \left(\sum_j F_{ij} \right) < 1. \qquad (2.31)$$

However, the spectral radius $\rho(F)$, which is the maximal eigenvalue modulus of F, cannot exceed its norm [12]

$$0 < \rho(F) \leq \|F\| = (1 - \min\{f_{k1} + f_{k2} : 3 \leq k \leq n\}) < 1, \qquad (2.32)$$

where n is the total number of levels. This guarantees the convergence of the power series in F, since

$$\lim_{N \to \infty} \{\rho(F)\}^N = 0, \qquad (2.33)$$

and F is related to its Jordan canonical form by a similarity transformation [12]. We now estimate the fractional error in our approximation using the ratio

$$\frac{\|F_\infty - F_N\|}{\|F_\infty\|} = \frac{\|F^N + F^{N+1} + F^{N+2} + \cdots\|}{\|F_\infty\|}$$

$$= \frac{\|F^N(I + F + F^2 + \cdots)\|}{\|F_\infty\|}$$

$$= \frac{\|F^N F_\infty\|}{\|F_\infty\|} \leq \frac{\|F^N\| \|F_\infty\|}{\|F_\infty\|}$$

$$= \|F^N\|, \tag{2.34}$$

where we have used the inequality

$$\|F_1 F_2\| \leq \|F_1\| \|F_2\| \tag{2.35}$$

for any two $m \times m$ matrices F_1 and F_2 [12]. We may also use this inequality to note that $\|F^N\| \leq \|F\|^N$. However, the row sum of the substochastic matrix F is maximized for the row k in the parent matrix corresponding to a minimum in the sum $(f_{k1} + f_{k2})$ of branching ratios to the ground and metastable states. For $T_9 \leq 10.0$, this is of the order 10^{-17} to 10^{-15}. Thus while $\|F\|^N$ is certainly an upper bound on $\{\rho(F)\}^N$, in practice it is too conservative to be used as a convergence criterion. We have used $\|F^N\|$ to estimate the fractional error. As will be seen in Sec. IV, it turns out to be an excellent guide.

III. A COMBINATORIAL INTERPRETATION OF THE EFFECTIVE RATE

The expression enclosed by square brackets in Eq. (2.29) is actually the effective branching ratio ($= f_{21}^{eff}$) due to indi-

rect transitions. Let each nuclear energy level be represented by the node of a directed graph (digraph), weighted such that the transition probability f_{ij} is the cost of the arc connecting nodes i and j. If the costs of successive arcs along a path are combined multiplicatively to yield the path cost, then Eq. (2.29) is the *transfer matrix* formula for the sum of the costs of all possible paths between nodes 2 and 1, with the restriction that the number of intermediate nodes should not exceed N. (See Ref. [13] and references therein for a detailed discussion of the transfer matrix in graph theory.) In other words, our technique is a combinatorial *enumeration* of all finite "f strings" of the form $(f_{2i_1} f_{i_1 i_2} f_{i_2 i_3} \cdots f_{i_m 1})$, where $1 \leq m \leq N$.

Suppose we wish to find the effective rate to order $N = 3$ for a $n = 4$ level system. First we need the $(n-2) \times (n-2)$ matrix F, which reduces to order 2×2,

$$F = \begin{pmatrix} 0 & f_{34} \\ f_{43} & 0 \end{pmatrix}. \tag{3.1}$$

Next we compute the partial sum of transfer matrices

$$F_N = F_3 = I + F + F^2 = \begin{pmatrix} 1 + f_{34}f_{43} & f_{34} \\ f_{43} & 1 + f_{43}f_{34} \end{pmatrix}. \tag{3.2}$$

The effective rate to third order in the series expansion may then be obtained immediately from Eq. (2.29),

$$\lambda_{21,3}^{eff} = \Lambda_2 \left\{ (f_{23}f_{24}) \begin{pmatrix} 1 + f_{34}f_{43} & f_{34} \\ f_{43} & 1 + f_{43}f_{34} \end{pmatrix} \begin{pmatrix} f_{31} \\ f_{41} \end{pmatrix} \right\} \tag{3.3}$$

$$= \Lambda_2 (\underbrace{f_{23}f_{31} + f_{24}f_{41}}_{\text{all two-arc paths}} + \underbrace{f_{23}f_{34}f_{41} + f_{24}f_{43}f_{31}}_{\text{all three-arc paths}} + \underbrace{f_{23}f_{34}f_{43}f_{31} + f_{24}f_{43}f_{34}f_{41}}_{\text{all four-arc paths}}).$$

$$\underbrace{\phantom{f_{23}f_{31} + f_{24}f_{41} + f_{23}f_{34}f_{41} + f_{24}f_{43}f_{31} + f_{23}f_{34}f_{43}f_{31} + f_{24}f_{43}f_{34}f_{41}}}_{\text{effective branching ratio}} \tag{3.4}$$

Keeping in mind that the number of arcs in a path is one more than the number of intermediates visited between the origin and the destination, we see from Eq. (3.4) that Eq. (2.29) automatically enumerates every possible pathway with 1, 2 or 3 intermediate nodes. The matrix F_N elegantly enumerates all the ways in which nodes 3 and 4 can be arranged to give 1, 2, and 3 intermediates. Then $(f_2^{out})^T$ connects the possible "intermediate circuits" to the metastable state to "feed" them while at the other end f_1^{in} connects them to the ground state, which is the final "recipient." Though a strictly

correct calculation of λ_{21}^{eff} would use F_∞, F_N typically converges rapidly for finite N because the magnitude of every element of F is strictly less than unity.

Further insight may be obtained by defining the following:

(i) The N-arc "cascade probability vectors"

$$\Gamma_{q,N}^{in} = \begin{pmatrix} \Gamma_{3q} \\ \vdots \\ \Gamma_{nq} \end{pmatrix} \equiv F_N f_q^{in}.$$

Ultimately, all the short-lived upper-lying levels must decay to the ground ($q=1$) or the metastable ($q=2$) states. However, unlike the normal use of the word "cascade" where the transitions are exclusively downward, we also allow intermediate "up" transitions. Given a maximum of N intermediate levels, Γ_{k1} is the effective probability that level k ($k \geq 3$) will ultimately decay to the ground state, while Γ_{k2} is the probability of its ultimate decay to the metastable state. It will be shown that $\Gamma_{k1} + \Gamma_{k2} = 1$, as expected;

(ii) The N-arc generalization of f_q^{out} ($q = 1,2$), which is

$$\Gamma_{q,N}^{out} = \begin{pmatrix} \Gamma_{q3} \\ \vdots \\ \Gamma_{qn} \end{pmatrix} \equiv F_N^T f_q^{out};$$

(iii) The "reverse ratio" $R_{ij} = (\lambda_{ij}/\lambda_{ji}) = (Y_j^{eq}/Y_i^{eq})$, where Y_k^{eq} is the equilibrium abundance of level k and detailed balance has been invoked;

(iv) The diagonal "reverse ratio matrix" R_q with elements $(R_q)_{ij} = \delta_{ij} R_{qi}$, where $3 \leq i,j \leq n$; and

(v) The diagonal matrix $S_q \equiv (1/\Lambda_q)\Lambda R_q$, where Λ is the destruction matrix defined previously. The elements of S_q are $(S_q)_{ij} = (\Lambda_i R_{qi} \delta_{ij}/\Lambda_q)$, where $3 \leq i,j \leq n$.

With these definitions, we have

$$(\Lambda F \Lambda^{-1})_{il} = \sum_{j,k} \Lambda_j \delta_{ij} F_{jk} \Lambda_k^{-1} \delta_{kl}. \tag{3.5}$$

But,

$$F_{jk} = f_{jk} = \frac{\lambda_{jk}}{\Lambda_j} = \frac{R_{jk}\lambda_{kj}}{\Lambda_j} = \frac{R_{jk}f_{kj}\Lambda_k}{\Lambda_j}. \tag{3.6}$$

Substituting Eq. (3.6) into Eq. (3.5), we have

$$(\Lambda F \Lambda^{-1})_{il} = \sum_{j,k} \delta_{ij} R_{jk} f_{kj} \delta_{kl} = R_{il} f_{li}, \tag{3.7}$$

which immediately allows us to show that $S_q F S_q^{-1} = F^T$, as follows:

$$(S_q F S_q^{-1})_{il} = \sum_{j,k} \frac{1}{\Lambda_q} R_{qj} \delta_{ij} (\Lambda F \Lambda^{-1})_{jk} \Lambda_q R_{kq} \delta_{kl}$$

$$= \sum_{j,k} R_{kj} \delta_{ij} R_{jk} f_{kj} \delta_{kl}$$

$$= \sum_{j,k} R_{kj} R_{jk} \delta_{ij} f_{kj} \delta_{kl} = f_{li}. \tag{3.8}$$

Recall that F is the transfer matrix. It gives the probabilities for the upper-lying level abundances to rearrange themselves via one arc. This "rearrangement" may be thought of as a flow of abundance among the upper-lying levels. The operator $F^{\mathbf{T}}$, then, gives the flow in the opposite direction; therefore, S_q may be considered the representation of a path-reversal operator.

Because F is transposed by a similarity transformation under S_q, so is any power of F,

$$S_q F^m S_q^{-1} = \underbrace{S_q F S_q^{-1} S_q F S_q^{-1} \cdots S_q F S_q^{-1}}_{m \text{ repetitions}} = (F^T)^m. \tag{3.9}$$

Hence, we conclude that the similarity transformation also holds for F_N,

$$S_q F_N S_q^{-1} = S_q(I + F + F^2 + \cdots + F^{N-1}) S_q^{-1}$$

$$= I + F^T + (F^T)^2 + \cdots + (F^T)^{N-1} = F_N^T. \tag{3.10}$$

From Eq. (3.10) we obtain

$$S_q F_N = F_N^T S_q \tag{3.11}$$

or

$$S_q F_N f_q^{in} = F_N^T S_q f_q^{in}. \tag{3.12}$$

But,

$$(S_q f_q^{in})_i = \frac{\Lambda_i f_{iq} R_{qi}}{\Lambda_q} = \frac{\lambda_{iq} R_{qi}}{\lambda_q} = f_{qi}, \tag{3.13}$$

i.e.,

$$S_q f_q^{in} = f_q^{out}. \tag{3.14}$$

We substitute Eq. (3.14) into Eq. (3.12) to obtain

$$S_q F_N f_q^{in} = F_N^T f_q^{out} \tag{3.15}$$

or

$$S_q \Gamma_q^{in} = \Gamma_q^{out}. \tag{3.16}$$

The results in Eqs. (3.10), (3.14), and (3.16) further confirm the interpretation of S_q as a representation of the path-reversal operator for all orders. Expressing Eq. (2.29) in our new notation,

$$\lambda_{21}^{eff} = \Lambda_2(f_2^{out})^T \Gamma_1^{in}$$

$$= \Lambda_2(f_2^{in})^T S_2^T S_1^{-1} \Gamma_1^{out}. \tag{3.17}$$

However,

$$(S_2^T S_1^{-1})_{ij} = \delta_{ij} \frac{1}{\Lambda_2} \Lambda_i R_{2i} \frac{1}{\Lambda_i} \Lambda_1 R_{i1} = \delta_{ij} \frac{\Lambda_1}{\Lambda_2} R_{21}, \tag{3.18}$$

i.e.,

$$S_2^T S_1^{-1} = \frac{\Lambda_1}{\Lambda_2} R_{21} I. \tag{3.19}$$

Substituting Eq. (3.19) into Eq. (3.17) we find that

$$\lambda_{21}^{eff} = R_{21}\frac{\Lambda_1}{\Lambda_2}\Lambda_2(f_2^{in})^T\Gamma_1^{out}$$

$$= R_{21}\Lambda_1(f_2^{in})^T\Gamma_1^{out}$$

$$= R_{21}\Lambda_1(\Gamma_1^{out})^T f_2^{in} = R_{21}\lambda_{12}^{eff}. \tag{3.20}$$

Hence it is true that $(\lambda_{21}^{eff}/\lambda_{12}^{eff}) = (\lambda_{21}/\lambda_{12}) = R_{21}$ for any number of levels n and any number of intermediates m, thus ensuring that our effective rates will always result in the correct equilibrium abundance ratio for the ground and metastable states, within the Nth order approximation.

We may also obtain further insight into the steady-state abundance vector by recasting Eq. (2.26) as

$$Y_N^{SS} = \Lambda^{-1}F_N^T(\Lambda_1 Y_1 f_1^{out} + \Lambda_2 Y_2 f_2^{out})$$

$$= \Lambda^{-1}\{\Lambda_1 Y_1 \Gamma_1^{out} + \Lambda_2 Y_2 \Gamma_2^{out}\}, \tag{3.21}$$

from which we extract the very revealing scalar equation

$$Y_k^{SS} = \frac{\Lambda_1\Gamma_{1k}Y_1 + \Lambda_2\Gamma_{2k}Y_2}{\Lambda_k}. \tag{3.22}$$

This result demonstrates that Eq. (3.21) is the multidimensional analog of Eq. (2.7). Similarly, the multidimensional effective rate derived in Eq. (2.29) may be expressed as

$$\lambda_{21}^{eff} = (\lambda_2^{out})^T(\Gamma_1^{in})$$

$$= (\lambda_{23} \cdots \lambda_{2n})\begin{pmatrix} \Gamma_{31} \\ \vdots \\ \Gamma_{n1} \end{pmatrix}, \tag{3.23}$$

which mirrors the scalar Eq. (2.17) perfectly as well.

Finally, we note that

$$\Gamma_{k1} + \Gamma_{k2} = \frac{\Lambda_1\Gamma_{1k}R_{k1}}{\Lambda_k} + \frac{\Lambda_2\Gamma_{2k}R_{k2}}{\Lambda_k} = \left(\frac{1}{Y_k^{eq}}\right)$$

$$\times\left\{\frac{(\Lambda_1\Gamma_{1k})Y_1^{eq} + (\Lambda_2\Gamma_{2k})Y_2^{eq}}{\Lambda_k}\right\} = 1, \tag{3.24}$$

since $R_{k1} = Y_1^{eq}/Y_k^{eq}$, $R_{k2} = Y_2^{eq}/Y_k^{eq}$, and the expression in braces is what the right-hand side of Eq. (3.22) would be at equilibrium, i.e., Y_k^{eq}. Thus, we have a simple proof of the fact that the probabilities to "cascade" from an upper-lying level to the ground and metastable states individually must sum to unity.

The language of path costs can be further exploited when we wish to identify the dominant pathway at a particular temperature. All we need do is to assign $(-\ln f_{ij})$ to the arc weights of a digraph and then use Dijkstra's *Shortest Path Algorithm* [14] to find the shortest path (with an additive combination of arc costs) between nodes 2 and 1. The path with the minimum sum of negative logarithms will be the same as the path with the maximal product of the f_{ij}. As we shall see in our discussion of ^{26}Al in Sec. IV, at low temperatures only a single path or "chain of f's" contributes to

the effective rate, while at high temperatures so many paths are open to the system that the concept of a dominant path is meaningless. The shortest path concept can easily be extended to finding the percentage contributions of different paths to the total effective rate by using a kth shortest path algorithm.

We conclude this section with a summary of the algorithmic content of the foregoing discussion.

Step One. Construct the substochastic transfer matrix F of transition probabilities at a particular temperature by excluding transitions to and from both the ground and metastable states. That is, the elements of the $(n-2)\times(n-2)$ matrix F are the branching ratios f_{ij} given by Eq. (2.14) for the range $3 \leq i,j \leq n$, where n is the total number of levels in the system.

Step Two. Compute the partial sum $F_N = I + F + F^2 + F^3 + \cdots + F^{N-1}$, truncating the series expansion when $\|F^N\|$, which is a bound on the fractional error, reaches an acceptably small value.

Step Three. Calculate the effective rates $\lambda_{21,N}^{eff} = \Lambda_2(f_2^{out})^T F_N f_1^{in}$ and $\lambda_{12,N}^{eff} = \Lambda_1(f_1^{out})^T F_N^T f_2^{in}$, where f_q^{out} is defined in the discussion just preceding Eq. (2.22), and f_q^{in} in Eq. (2.27). Here, Λ_1 and Λ_2 are the total destruction rates, as defined by Eq. (2.6), out of the ground and metastable states, respectively. This procedure may be repeated for a discrete set of temperatures and a smooth curve fitted to the resulting points to obtain analytic expressions for the effective rates as functions of temperature.

IV. APPLICATION TO ^{26}Al

We now apply the combinatorial enumeration technique discussed in the previous two sections to the specific case of ^{26}Al. Figure 1 shows a log-log plot of λ_{21}^{eff} for the ^{26}Al internal equilibration as a function of temperature. To compute this rate, we used experimental data downloaded using the "Isotope Explorer" program from the Evaluated Nuclear Structure Data File website maintained by Brookhaven National Laboratories. Rates between 67 nuclear levels of the isotope were entered, with the highest level at $E_x = 6084$ keV. Rate information for levels above this energy was virtually nonexistent. At temperatures where other transition rates compete with the internal equilibration, very few photons in the stellar heat bath would have energies above 6 MeV, so the neglect of higher-lying levels is not too important. We study this in some detail below.

Theoretical single-particle rates (Weisskopf estimates) have been used for all spontaneous rates not known from experiment, with the exception of λ_{32}^{spont} and λ_{42}^{spont}, for which we used the results of shell-model calculations (obtained from Refs. [9,15]). The dashed line differs from the solid line only in that λ_{32}^{spont} was set to zero. At low temperatures, the drastic difference between the two curves illustrates how our lack of experimental data for a particular level may impact a calculation of the effective rate. However, the matrix series approach provides an excellent diagnostic for such levels, since by zeroing out the row and column pertaining to a particular level we may ascertain its importance
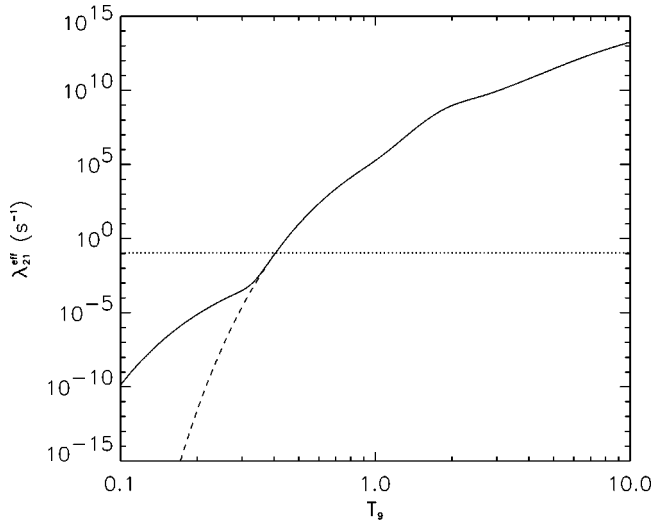
FIG. 1. The effective transition rate λ_{21}^{eff} for ^{26}Al as a function of temperature. The solid line gives the result of the full calculation. The dashed line gives the rate when the direct transitions between levels 2 and 3 are disabled. For reference, the dotted line gives the β^+-decay rate of the 0^+ metastable state. For $T_9 \lesssim 0.4$, the metastable state has no chance of equilibrating with the ground state before β decaying.

in the overall equilibration rate.

The strongest single-particle transitions occur between two nuclear levels when their spins differ by zero or unity and when their parities are different, since the selection rules permit $E1$ transitions to occur. However, at low temperatures such transitions are hampered in ^{26}Al by the fact that in our set of 67 levels, every energy level below 4.4 MeV has positive parity. Thus the system is forced to make small spin jumps with no change in parity. Figure 2 shows the dominant paths at five different temperatures. Below $T_9 \approx 0.3$ the transition through the levels $2-3-1$ completely dominates the scenario. This represents a $0^+ - 3^+ - 5^+$ progression in spins and parities. At $T_9 = 0.6$ the dominant route is through levels $2-4-3-1$ where the spin-parity progression is $0^+ - 1^+ - 3^+ - 5^+$. With the opportunity to reach for higher energy levels that may offer even smaller spin increments, we have at $T_9 = 1.3$ the level route $2-4-8-3-1$ with a spin-parity chain $0^+ - 1^+ - 2^+ - 3^+ - 5^+$. This progression dominates until $T_9 \approx 3.0$ when several 2^- states at ~ 4.5 MeV become accessible, allowing parity changes. This is reflected in the fourth pathway in Fig. 2. The fifth pathway in Fig. 2 through the levels $2-4-35-3-36-1$ is the dominant one at $T_9 = 5.0$: it has a $0^+ - 1^+ - 2^- - 3^+ - 4^+ - 5^+$ progression with all spin jumps equal to unity. At this temperature there are so many optimal paths that the concept of one best route becomes meaningless. This is illustrated by Fig. 3 which shows the steep drop in the contribution of the dominant path to the total effective rate as a function of temperature. The five most dominant pathways in the internal equilibration of ^{26}Al at $T_9 = 5.0$ are shown in Fig. 4. The most dominant pathway starts furthest to the left. The second, third, fourth, and fifth most dominant pathways start sequentially rightward of the most dominant and are minor variations of it.

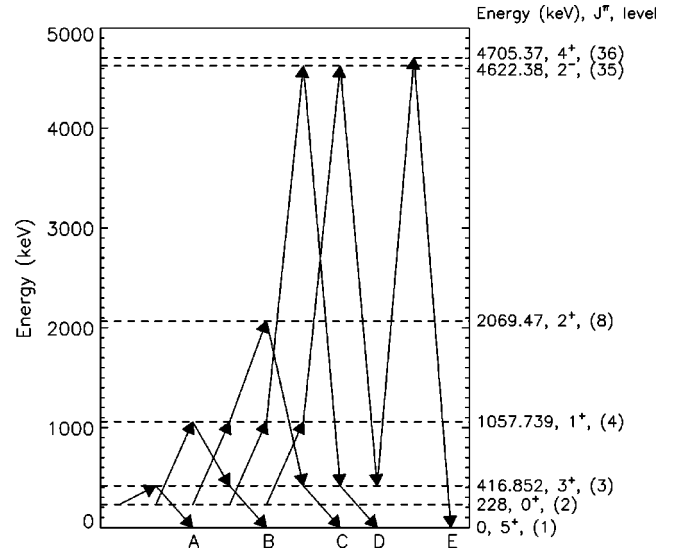We now discuss issues of convergence. Figure 5 shows

FIG. 2. The dominant pathways at (A) $T_9 = 0.2$, (B) $T_9 = 0.6$, (C) $T_9 = 1.3$, (D) $T_9 = 3.0$, and (E) $T_9 = 5.0$ in the internal equilibration of ^{26}Al. At low temperatures, the dominant pathways must take spin jumps larger than unity. At higher temperatures, large energy transitions are possible. This allows strongly favored spin jumps of unity in the dominant pathway, thereby dramatically increasing the effective equilibration rates. Levels are denoted by the format, energy in keV, spin parity, and (level number) on the right-hand side of the energy-level diagram.

the number of terms that we must retain to attain an accuracy of one part in 10^{16}. Figure 6 demonstrates the effect of considering a finite number of nuclear energy states. It is clear that a single intermediate node (level 3, which is a 3^+ at 0.416 MeV) suffices until we reach $T_9 \approx 0.3$. Thereafter, higher energy levels and multiple intermediate nodes become necessary as rising temperatures make more complicated pathways energetically possible. Four energy levels (level 4 is a 1^+ state at 1.058 MeV) and two intermediate nodes suffice until $T_9 \approx 1.0$. Beyond $T_9 \approx 1.0$, the number of terms
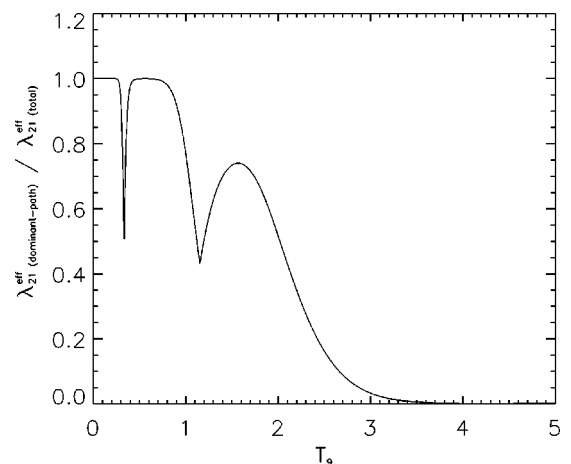

FIG. 3. Fractional contribution of the dominant pathway to the total rate λ_{21}^{eff} in ^{26}Al. When this quantity is unity, a single pathway dominates the effective rate. Clearly different regimes apply at different temperatures. These are identified in the text in Sec. IV.
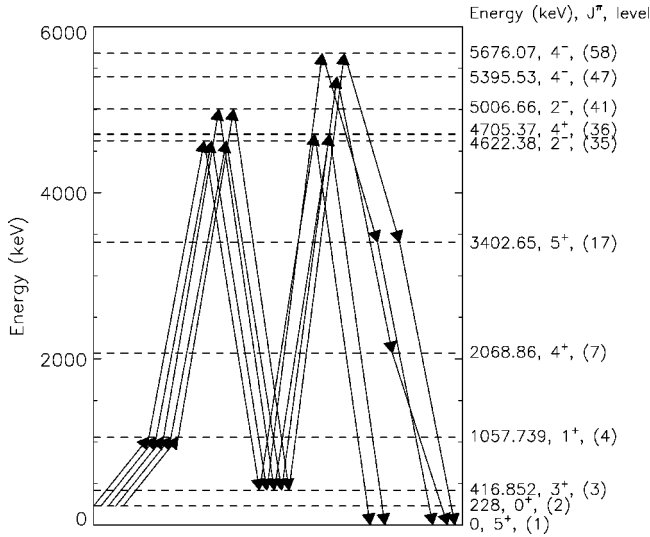
FIG. 4. The first five dominant pathways in the internal equilibration of ^{26}Al at $T_9 = 5.0$. The most dominant pathway is the one that starts furthest to the left. The second, third, fourth, and fifth most dominant pathways start sequentially rightward of the most dominant.

FIG. 6. Variations in the effective flow rate from the metastable-state ensemble to the ground-state ensemble when a different number of nuclear energy levels is used to approximate the full network. The rates are accurate to one part in 10^{16} for the adopted level subset.

in the expansion, which had stayed almost constant, begins to show a very steep increase indicating the onset of very complex pathways. However, at all temperatures the number of terms required is finite. At $T_9 = 2.0$, the number of terms required in the matrix series is $N = 74$. At $T_9 = 5.0$, 1239 terms are required in the matrix series, and at $T_9 = 10.0$, $N = 22\,332$. Even the last calculation imposes very mild demands on computer time. The effect of *not* including enough terms, however, is quite dramatic. As Fig. 5 shows, an inadequate number of transit points in the flow from the ground-state ensemble to the metastable-state ensemble can result in pathological behavior in the vicinity of $T_9 = 3.0$ where the rate curves actually dip below values attained at lower temperatures. This happens because many higher-lying levels open up at such high temperatures, but if we constrain the
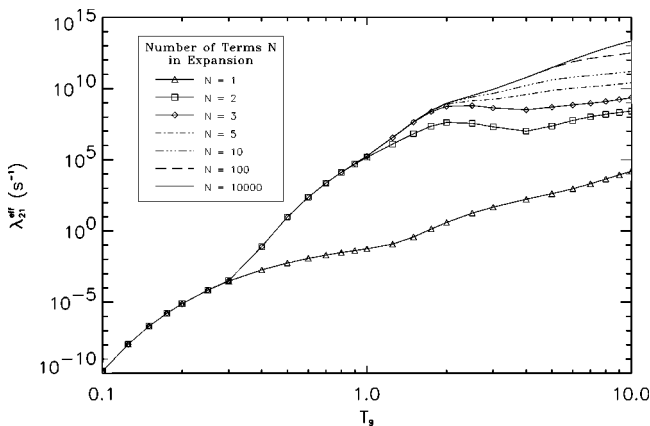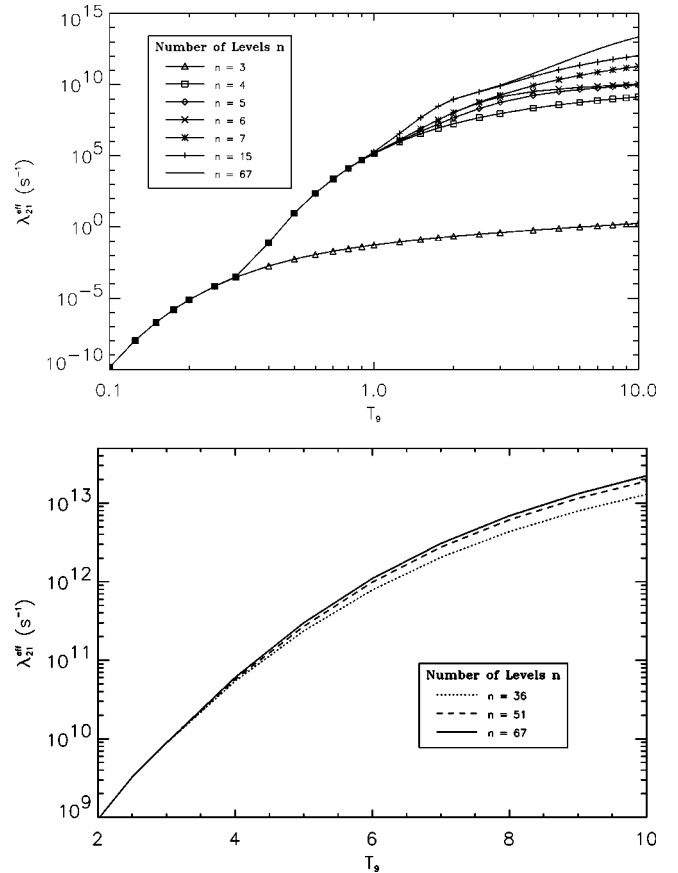

FIG. 5. Variations in the effective flow rate from the metastable-state ensemble to the ground-state ensemble when a different number of terms is retained in the series expansion. The rates are accurate to one part in 10^{16}.

system to an inadequate number of intermediate nodes then it cannot take advantage of the pathways that have become available. Indeed, since the f_{ij}'s among the lower-lying levels *decrease* with rising temperature, the rate as a whole suffers a decline due to premature series truncation.

Table I investigates the dependability of $\|F^N\|$ as a convergence criterion. Clearly, the general trend of increase in N with temperature is closely followed for the different accuracies (one part in $10^{16}, 10^{10}, 10^6, 10^3, 10^2$, and 10^1). In fact, at a fixed temperature N varies remarkably slowly even though we investigate such a wide range of accuracies. Indeed, we have observed that 90% accuracy is achieved in the rate calculation when an accuracy of one part in 10 is estimated by $\|F^N\|$, 99% accuracy for one part in 10^2, and so on. This interesting result may be obtained by comparison with rates for $N = 1\,000\,000$, at which the last term of the matrix series is zero for the purpose of practical computation. This indicates that even though $\|F^N\|$ is a conservative estimate of the fractional error, it is a very good one. It behaves like a "least upper bound," loosely speaking, and is a powerful tool for ensuring not only the accuracy of our technique, but also its efficiency, since it curtails superfluous matrix arithmetic. Such is not the case for $\|F\|^N$, which for the reasons discussed in Sec. II grossly overestimates the fractional error

TABLE I. The number of terms to be retained in the series expansion for different accuracies. The convergence criterion $s \equiv \|F^N\|$ bounds the fractional error caused by series truncation at the Nth partial sum for the chosen temperatures.

T_9	$s=10^{-16}$	$s=10^{-10}$	$s=10^{-6}$	$s=10^{-3}$	$s=10^{-2}$	$s=10^{-1}$
0.0100	12	10	9	7	6	6
0.0125	12	10	9	7	6	6
0.0150	12	10	9	7	6	6
0.0175	12	10	9	7	6	6
0.0200	12	10	9	7	6	6
0.0250	12	10	9	7	6	6
0.0300	12	10	9	7	6	6
0.0400	12	10	9	7	6	6
0.0500	12	10	9	7	6	6
0.0600	12	10	9	7	6	6
0.0700	12	10	9	7	6	6
0.0800	12	10	9	7	6	6
0.0900	12	10	9	7	6	6
0.1000	12	10	9	7	6	6
0.1250	12	10	9	7	6	6
0.1500	12	10	9	7	6	6
0.1750	12	10	9	7	6	6
0.2000	12	10	9	7	6	6
0.2500	13	10	9	7	6	6
0.3000	13	11	9	7	6	6
0.4000	14	11	9	7	6	6
0.5000	16	12	9	7	6	6
0.6000	17	12	9	7	6	6
0.7000	18	13	10	7	6	6
0.8000	20	14	10	7	6	6
0.9000	22	15	11	8	7	6
1.0000	23	16	11	8	7	6
1.2500	28	19	13	8	7	6
1.5000	34	23	15	9	8	6
1.7500	46	30	20	12	9	7
2.0000	74	48	30	17	13	8
2.5000	190	120	74	39	27	16
3.0000	359	226	137	71	49	27
4.0000	661	415	251	128	87	46
5.0000	1239	777	469	237	160	83
6.0000	2862	1791	1077	542	363	185
7.0000	6140	3840	2306	1156	773	389
8.0000	10989	6870	4124	2065	1378	692
9.0000	16671	10421	6255	3130	2089	1047
10.0000	22332	13959	8378	4192	2796	1401

and turns out to be utterly useless as a convergence criterion, since it asks for $\sim 10^{15}$ to 10^{17} terms over the temperature range we consider.

Next, we consider the effect of including only a finite number n of discrete energy states. Varying n is tantamount to redefining the effective infinite energy of the system, and consequently the effective rate plateaus at a temperature that depends on n, as can be seen in Fig. 6. Thus we see a smooth leveling off of the effective rate at different temperatures for

$n=3$, $n=4$, $n=5$ and so on, rather than the dips and kinks due to premature series truncation in Fig. 5. The effective rates smoothly approach the $n=67$ curve, with major changes only at $n=17$ and $n=36$. These are levels that redefine the limit energy of the system at $T_9 \approx 3.0$ and $T_9 \approx 4.0$, respectively, when rising temperature allows the system to access higher energy states, if any are available. We conclude that $n=67$ does indeed institute a satisfactory limit point over the range of temperatures we consider ($T_9 \leqslant 10.0$).

At this point, we note that it would be possible in principle to include higher-lying states through the use of a theoretical nuclear level density. In practice, such a level density would be a continuous function of excitation energy in the nucleus. Our technique, however, discretizes the energy grid, so we would likely group levels into energy bins. We intend to explore this approach in future work.

Finally, since those rates not obtained from experiment were calculated using the Weisskopf single-particle estimates, we have most certainly incorrectly estimated some of the individual transition rates. This leads us to conduct a sensitivity analysis, since large dependencies of the effective rates on many individual transitions would cast doubt on the robustness of our results. Table II shows the enhancement in the overall effective rate when an individual transition is enhanced by a factor of 100. Transitions that cause enhancements by less than a factor of 1.1 (i.e., 10%) in the overall rate have not been included in Table II. Similarly, Table III shows the factor by which the overall effective rate decreases when an individual transition is suppressed by a factor of 100. The decrease factor is taken as the ratio of the overall effective rate to the effective rate with a decrease in the individual transition rate. Transitions with decrease factors less than 1.11 (i.e., reductions that still leave more than 90% of the original value) in the overall rate have been omitted from Table III. We can immediately see that very few individual transitions have any appreciable impact on the effective rate, and that while perturbations in the destruction rates out of levels 3 and 4 can scale almost linearly in the rate at low temperatures (since they are the only levels participating), such dramatic correlations are rare for the other levels. In particular, we note from Table III that the suppression factors for the effective rate are very close to one (except for transitions out of levels 3 and 4) and thus our use of Weisskopf estimates is unlikely to lead to errors in the effective rates greater than a few tens of percent.

V. THE APPROACH TO EQUILIBRIUM

The results of the previous sections permit not only a calculation of the effective equilibration rate between the ground and metastable states but also insights into how that equilibration occurs. This issue is most easily explored using a quantity analogous to the fugacity of a phase.

In any study of equilibration, one follows ensembles of different species in contact with each other. In a study of the internal equilibration of an isotope, the different species are its various isomers at different excitation energies E_i for level i. In keeping with usual practice in nucleosynthesis

TABLE II. Factor by which the effective rate increases when the rate for the indicated spontaneous transition is enhanced by a factor of 100. Only those transitions that show an increase or decrease of 10% or greater for one of the indicated temperatures are presented. The transition from level i to level j is identified in the form $i \rightarrow f$. The important levels are level 1 (ground state, 5^+), level 2 (metastable state, 0.228 MeV, 0^+), level 3 (0.417 MeV, 3^+), level 4 (1.058 MeV, 1^+), level 7 (2.069 47 MeV, 2^+), level 8 (2.071 64 MeV, 1^+), level 17 (3.042 MeV, 5^+), and level 36 (4.705 MeV, 4^+).

Transition	T_9																							
	0.01	0.15	0.20	0.30	0.40	0.50	0.60	0.70	0.80	0.90	1.00	1.50	2.00	2.50	3.00	3.50	4.00	4.50	5.00	6.00	7.00	8.00	9.00	10.00
(3 → 1)	1.00	1.00	1.00	1.00	1.00	1.00	1.00	1.00	1.00	1.00	1.00	1.04	1.73	4.50	7.85	8.65	6.45	4.13	2.72	1.57	1.23	1.11	1.06	1.04
(3 → 2)	100.00	100.00	100.00	92.24	3.32	1.06	1.00	1.00	1.00	1.00	1.00	1.00	1.00	1.00	1.00	1.00	1.00	1.00	1.00	1.00	1.00	1.00	1.00	1.00
(4 → 2)	1.00	1.00	1.00	1.00	1.00	1.00	1.00	1.00	1.00	1.00	1.00	1.00	1.00	1.00	1.00	1.00	1.00	1.01	1.01	1.03	1.06	1.10	1.14	1.17
(4 → 3)	1.00	1.00	1.00	8.74	97.50	99.76	99.77	99.42	97.57	90.93	75.41	6.48	1.43	1.05	1.01	1.00	1.00	1.00	1.00	1.00	1.00	1.00	1.00	1.00
(7 → 1)	1.00	1.00	1.00	1.00	1.00	1.00	1.00	1.00	1.00	1.00	1.00	1.00	1.07	1.72	3.15	5.28	8.01	10.54	11.79	10.06	7.02	4.99	3.82	3.13
(8 → 2)	1.00	1.00	1.00	1.00	1.00	1.00	1.00	1.00	1.00	1.01	1.04	1.16	1.10	1.03	1.01	1.01	1.00	1.00	1.01	1.01	1.02	1.04	1.06	1.07
(8 → 3)	1.00	1.00	1.00	1.00	1.00	1.00	1.00	1.01	1.04	1.19	1.59	3.39	1.73	1.17	1.06	1.03	1.01	1.00	1.00	1.00	1.00	1.00	1.00	1.00
(8 → 4)	1.00	1.00	1.00	1.00	1.00	1.00	1.00	1.00	1.00	1.01	1.05	1.21	1.12	1.04	1.01	1.01	1.00	1.00	1.00	1.00	1.00	1.00	1.00	1.00
(17 → 1)	1.00	1.00	1.00	1.00	1.00	1.00	1.00	1.00	1.00	1.00	1.00	1.00	1.00	1.00	1.01	1.08	1.31	1.80	2.52	3.98	4.62	4.50	4.13	3.79
(36 → 1)	1.00	1.00	1.00	1.00	1.00	1.00	1.00	1.00	1.00	1.00	1.00	1.00	1.00	1.01	1.10	1.48	2.27	3.35	4.44	5.77	5.79	5.23	4.64	4.21

TABLE III. Factor by which the effective rate decreases when the rate for the indicated spontaneous transition is suppressed by a factor of 100. Only those transitions that show an increase or decrease of 10% or greater for one of the indicated temperatures are presented. The transition from level i to level j is identified in the form $i \rightarrow f$. The important levels are level 1 (ground state, 5^+), level 2 (metastable state, 0.228 MeV, 0^+), level 3 (0.417 MeV, 3^+), level 4 (1.058 MeV, 1^+), level 7 (2.069 47 MeV, 2^+), level 8 (2.071 64 MeV, 1^+), level 17 (3.042 MeV, 5^+), and level 36 (4.705 MeV, 4^+).

Transition	T_9																							
	0.01	0.15	0.20	0.30	0.40	0.50	0.60	0.70	0.80	0.90	1.00	1.50	2.00	2.50	3.00	3.50	4.00	4.50	5.00	6.00	7.00	8.00	9.00	10.00
(3→1)	1.00	1.00	1.00	1.00	1.00	1.00	1.00	1.00	1.00	1.01	1.03	3.68	6.08	2.52	1.46	1.17	1.08	1.04	1.02	1.01	1.00	1.00	1.00	1.00
(3→2)	100.00	100.00	100.00	11.42	1.02	1.00	1.00	1.00	1.00	1.00	1.00	1.00	1.00	1.00	1.00	1.00	1.00	1.00	1.00	1.00	1.00	1.00	1.00	1.00
(4→2)	1.00	1.00	1.00	1.00	1.00	1.00	1.00	1.00	1.00	1.00	1.00	1.02	1.06	1.05	1.05	1.06	1.07	1.08	1.10	1.14	1.17	1.18	1.17	1.15
(4→3)	1.00	1.00	1.00	1.08	30.11	94.38	96.70	76.60	34.28	11.10	4.21	1.07	1.01	1.00	1.00	1.00	1.00	1.00	1.00	1.00	1.00	1.00	1.00	1.00
(7→ 1)	1.00	1.00	1.00	1.00	1.00	1.00	1.00	1.00	1.00	1.00	1.00	1.00	1.03	1.39	2.41	3.21	2.70	2.04	1.63	1.27	1.14	1.08	1.05	1.04
(8→3)	1.00	1.00	1.00	1.00	1.00	1.00	1.00	1.00	1.01	1.06	1.20	4.28	3.58	1.52	1.09	1.02	1.00	1.00	1.00	1.00	1.00	1.00	1.00	1.00
(8→4)	1.00	1.00	1.00	1.00	1.00	1.00	1.00	1.00	1.01	1.05	1.16	2.69	2.22	1.34	1.09	1.02	1.01	1.00	1.00	1.00	1.00	1.00	1.00	1.00
(17→1)	1.00	1.00	1.00	1.00	1.00	1.00	1.00	1.00	1.00	1.00	1.00	1.00	1.00	1.00	1.02	1.07	1.16	1.26	1.32	1.32	1.26	1.20	1.16	1.13
(36→1)	1.00	1.00	1.00	1.00	1.00	1.00	1.00	1.00	1.00	1.00	1.00	1.00	1.00	1.00	1.00	1.02	1.06	1.12	1.19	1.32	1.40	1.44	1.45	1.45

theory, we consider Y_i to be the abundance in the ith isomeric state per nucleon in the system; therefore, the number density n_i of such isomers is $n_i = \rho N_A Y_i$, where ρ is the mass density and N_A is Avogadro's number. Furthermore, we may take the nuclei to be nonrelativistic and nondegenerate in the stellar plasma. Therefore, the chemical potential associated with energy level E_i in the nucleus is

$$\mu_i(T,\rho,Y_i) = mc^2 + E_i + kT \ln\left\{\frac{\rho N_A Y_i}{g_i}\left(\frac{2\pi\hbar^2}{mkT}\right)^{3/2}\right\},$$
(5.1)

where m is the mass of the nucleus in its ground state, c is the speed of light, k is Boltzmann's constant, g_i is the multiplicity of level i, and $2\pi\hbar$ is Planck's constant. In writing Eq. (5.1), we have assumed $E_i \ll mc^2$, which is certainly true in any stellar environment.

In the case of equilibration of levels within an ensemble of identical nuclei, we imagine the ensemble to be in contact with a large heat bath (the stellar plasma) at fixed volume. We may then compute at fixed temperature and mass density the change in the chemical potential,

$$\mu_i - \mu_i^{eq} = \int_{Y_i^{eq}}^{Y_i} d\mu_i(T,\rho,Y_i) = kT \ln\left(\frac{Y_i}{Y_i^{eq}}\right) = kT \ln \phi_i,$$
(5.2)

where μ_i^{eq} is the chemical potential at equilibrium. At this point, it is convenient to consider the fugacity, a measure of the tendency to escape from a chemical phase, since this is precisely the role of ϕ_i in Eq. (5.2). We recognize that ϕ_i is not the strictly correct definition of the fugacity, which has units of pressure and is a measure of the deviation from ideality, not necessarily from chemical equilibrium; nevertheless, we appropriate the term because of its usefulness. As the system evolves towards equilibrium, abundance "flees" those levels for which $\phi > 1$ and "escapes" into those levels for which $\phi < 1$. When two levels have the same fugacity, there is no thermodynamic advantage in fleeing from one of the levels to the other. Equilibrium obtains when all the nuclear levels attain a fugacity of one.

Following the internal equilibration of a nucleus, then, amounts largely to following the evolution of the fugacity of each energy level. To do this, we begin by defining the fugacity vector Φ of upper-lying levels in the nucleus,

$$\Phi = \begin{pmatrix} \phi_3 \\ \vdots \\ \phi_n \end{pmatrix}.$$
(5.3)

As we have argued, the upper-lying levels are in a steady state during most of the internal equilibration of the nucleus. While this is true, then, we may write

$$\Phi = EY^{SS},$$
(5.4)

where the elements of the matrix E are $E_{ij} = \delta_{ij}/Y_i^{eq}$, $3 \le i, j \le n$. From the steady-state abundances Y^{SS} in Eq. (3.21), we find

$$\Phi = \{E\Lambda^{-1}Y_1^{eq}\Lambda_1\}\Gamma_1^{out}\left(\frac{Y_1}{Y_1^{eq}}\right) + \{E\Lambda^{-1}Y_2^{eq}\Lambda_2\}\Gamma_2^{out}\left(\frac{Y_2}{Y_2^{eq}}\right).$$
(5.5)

Now, the product $(E\Lambda^{-1}Y_1^{eq}\Lambda_1) = S_1^{-1}$ because

$$(E\Lambda^{-1}Y_1^{eq}\Lambda_1)_{ij} = \frac{Y_1^{eq}\Lambda_1\delta_{ij}}{Y_i^{eq}\Lambda_i} = \frac{\Lambda_1\delta_{ij}}{\Lambda_i R_{1i}} = (S_1^{-1})_{ij},$$
(5.6)

where we have made use of the detailed balance argument that $(Y_i^{eq}/Y_1^{eq}) = R_{1i}$. By exactly similar arguments, $(E\Lambda^{-1}Y_2^{eq}\Lambda_2) = S_2^{-1}$. With these results, and Eq. (5.2) for levels 1 and 2, we find

$$\Phi = S_1^{-1}\Gamma_1^{out}\phi_1 + S_2^{-1}\Gamma_2^{out}\phi_2,$$
(5.7)

which on application of Eq. (3.16) becomes

$$\Phi = \Gamma_1^{in}\phi_1 + \Gamma_2^{in}\phi_2.$$
(5.8)

Equation (5.8) provides an interesting interpretation of the fugacities of the upper-lying levels. In particular, the fugacity of level k is

$$\phi_k = \Gamma_{k1}\phi_1 + \Gamma_{k2}\phi_2.$$
(5.9)

Thus the fugacity of level k is a linear combination of the fugacities of the ground and metastable states. The coefficients are the probabilities for level k to eventually decay to levels 1 and 2, respectively. When full equilibrium obtains, $\phi_1 = \phi_2 = \phi_k$, and we recover $\Gamma_{k1} + \Gamma_{k2} = 1$, which reinforces our interpretation of these Γ's as probabilities. Thus, for example, if $\Gamma_{k1} = 1$ and $\Gamma_{k2} = 0$, the steady state would require the ground state and level k to be fully in equilibrium with each other. In this case there would be no communication between levels 1 and 2 via level k. Such a case is unphysical because transitions between level k and another upper-lying level would prevent Γ_{k2} from ever being strictly zero in a stellar plasma. The more general case is that ϕ_k lies between ϕ_1 and ϕ_2.

We now consider the time evolution of the abundance Y_1 in light of the fugacities. From Eq. (2.19), the differential equation governing the time evolution of Y_1 in our system (under the assumption of a steady state in the upper-lying levels) may be written

$$\frac{dY_1}{dt} = -\sum_{k>2} \lambda_{1k}Y_1\left(1 - \frac{\lambda_{k1}Y_k}{\lambda_{1k}Y_1}\right).$$
(5.10)

We now use the detailed balance argument that $\lambda_{k1}/\lambda_{1k} = Y_1^{eq}/Y_k^{eq}$ to write

$$\frac{dY_1}{dt} = -\sum_{k>2} \lambda_{1k}Y_1\left(1 - \frac{\phi_k}{\phi_1}\right).$$
(5.11)

This equation shows that the contribution level k makes to the change in Y_1 is due both to the rate to go from level 1 to k and to the driving factor given by $(1 - \phi_k/\phi_1)$. The greater the difference in the relative fugacities of levels 1 and k, the
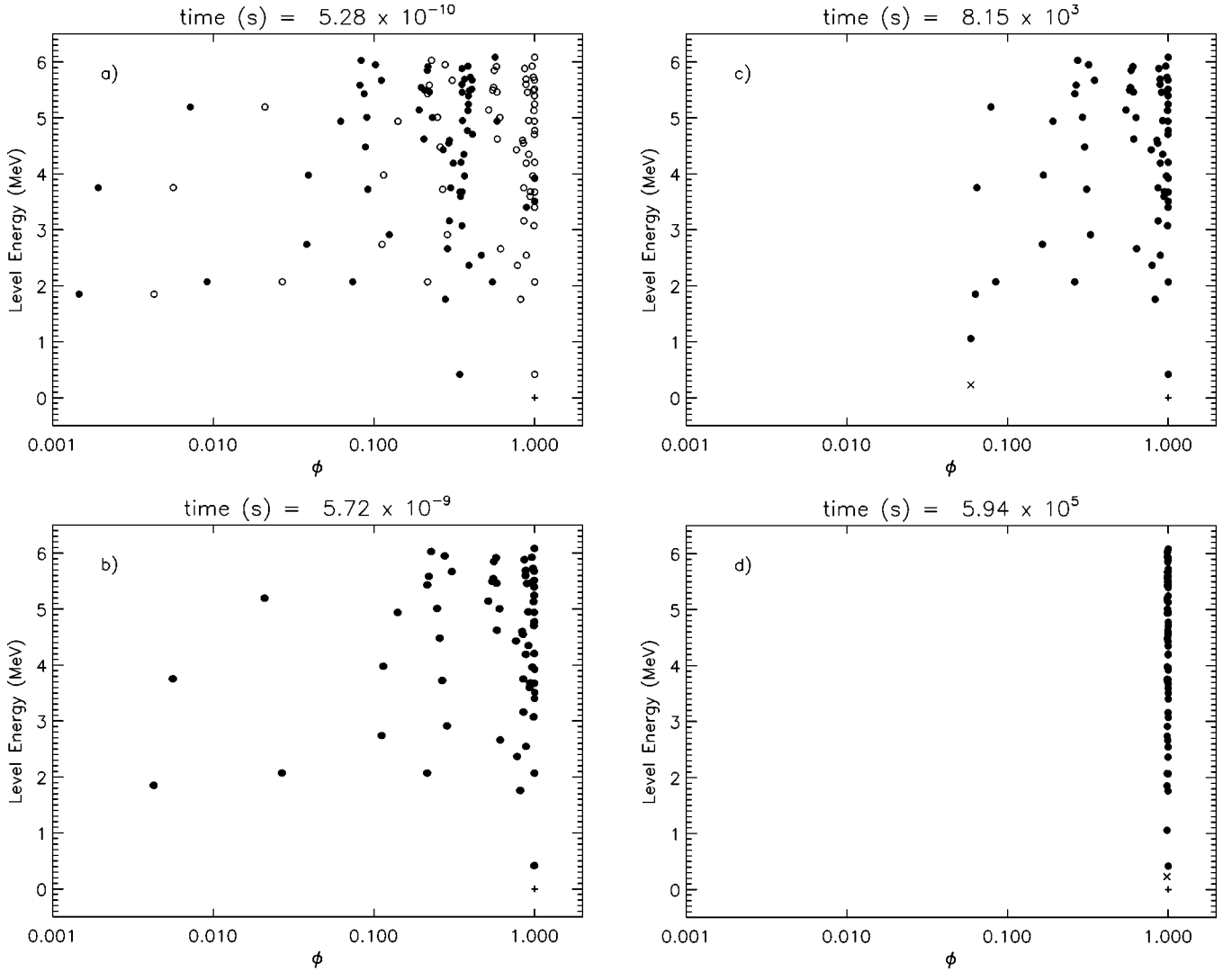
FIG. 7. Evolution of the fugacities ϕ for each level during the internal equilibration of ^{26}Al at $T_9 = 0.2$. The filled circles are the actual fugacities from the network calculation while the open circles give the fugacities derived from the steady-state abundances. The ''+'' gives the fugacity of the ground state while the "×" gives the fugacity for the metastable state (both are derived from the network abundances). The upper-lying levels reach a steady state early (within 5.72×10^{-9} ns), but equilibration does not occur until 6×10^5 s. This is far longer than the ~ 9 s decay time of the metastable state, so ^{26}Al cannot equilibrate at $T_9 = 0.2$. As discussed in Sec. V, once the upper-lying levels reach a steady state, their fugacities lie between those of the ground and metastable states. A given level k's fugacity is more closely tied to that of the ground or metastable state depending on its connections to them via Γ_{k1} or Γ_{k2}.

greater the driving factor. If levels 1 and k are in strict equilibrium, the driving factor for level k will be zero, leading to no change in Y_1. On the other hand, Eq. (5.9) shows that the maximum driving factor for any level is $(1 - \phi_2/\phi_1)$.

Substitution of Eq. (5.9) into Eq. (5.11) and use of $\Gamma_{k1} + \Gamma_{k2} = 1$ leads to

$$\frac{dY_1}{dt} = -\sum_{k>2} \lambda_{1k}\Gamma_{k2}Y_1\left(1 - \frac{\phi_2}{\phi_1}\right). \qquad (5.12)$$

With $\lambda_{1k} = \Lambda_1 f_{1k}$ we recognize Eq. (5.12) as

$$\frac{dY_1}{dt} = -\lambda_{12}^{eff}\left(1 - \frac{\phi_2}{\phi_1}\right)Y_1. \qquad (5.13)$$

If $\phi_1 > \phi_2$, then $1 - \phi_2/\phi_1 > 0$ and Y_1 will decrease with time. However, Y_1 will increase with time if $\phi_1 < \phi_2$. An analogous derivation yields

$$\frac{dY_2}{dt} = -\lambda_{21}^{eff}\left(1 - \frac{\phi_1}{\phi_2}\right)Y_2. \qquad (5.14)$$

These results show that it is the fugacity difference between levels 1 and 2 that drives the changes of Y_1 and Y_2. The changes cease once the ground and metastable states have equilibrated ($\phi_1 = \phi_2$).

Figure 7 shows the fugacities ϕ_k for the nuclear levels at four different times in the equilibration calculation for ^{26}Al at $T_9 = 0.2$. For the ground and metastable states the fugacities are those from the full network since they do not achieve

a steady state. Though the upper-lying levels do not begin in a steady state, it is clear they achieve this situation within 5.72×10^{-9} s. Because of the low temperature, the dominant transitions in ^{26}Al are downward spontaneous decays. The slowest of these is the decay of the 3^+ state at 0.417 MeV, which lives 1.25×10^{-9} and thereby governs the timescale to reach the steady state. In the subsequent evolution, the upper-lying levels remain in an excellently maintained steady state, as can be seen in Fig. 7. Final equilibrium is reached near 6×10^5 s. This is certainly long compared to the ~ 9 s beta-decay lifetime of the metastable state. Of course, this means the system would, in fact, never reach equilibrium because any ^{26}Al nuclei in the metastable state would decay before an equilibrium abundance could accumulate.

As expected from Eq. (5.9), the fugacity of the metastable state is always the least once the upper-lying levels go into a steady state while the fugacity of the ground state is always the greatest. This results from the fact that initially $Y_1 = 1$ and $Y_2 = 0$ so the net flow is from the ground to the metastable state. The situation would be reversed had the initial abundances been $Y_1 = 0$ and $Y_2 = 1$. The fugacities of the upper-lying levels lie between those of the ground and metastable states. It is clear that certain levels are more closely associated with the ground state than with the metastable state. This requires $\Gamma_{k1} \gg \Gamma_{k2}$. For example, the 3^+ level at 0.417 MeV has only a 1% branching to the 0^+ metastable state. This state links strongly to the ground state. By contrast, the 1^+ level at 1.058 MeV has only a 1.79×10^{-3}% branching to the 5^+ ground state. It links strongly to the metastable state. Interestingly, at $T_9 = 0.2$ most levels seem to be more strongly connected to the ground state than to the metastable state. As noted previously, the dominant transitions at this temperature tend to be the downward cascades, so these levels have fast transitions to the ground state or to another level with a fast transition to the ground.

The time taken to reach equilibrium (τ_{eq}) drops dramatically in the vicinity of $T_9 \sim 0.4$. At $T_9 = 0.5$, for instance, $\tau_{eq} = 0.6$ s, 5 orders of magnitude smaller than what it was at $T_9 = 0.2$. At $T_9 = 1.0$, $\tau_{eq} = 2.82 \times 10^{-5}$ s. Figure 8 shows the fugacities for each level at $T_9 = 2.0$ at four different times during the $T_9 = 2.0$ equilibration calculation, while Fig. 9 depicts the same for $T_9 = 5.0$. At these high temperatures, induced upward transitions become important. This has two interesting effects. First, the timescales for the ground and metastable states to reach a steady state are no longer much greater than those for the other levels. This means that the upper-lying levels are not in a steady state during a significant fraction of the period of growth of the metastable population. In this case, our steady-state treatment overestimates the abundance of the upper-lying levels and, hence, overestimates the rate of transfer from the ground to the metastable state. This is why the two-state system with effective rates evolves faster than the full network. The evolution is so fast at these high temperatures, however, and the competing processes probably so much slower that the error in using a two-state system is not likely to be of any significance.

The other interesting aspect of the high-temperature behavior is that once the system reaches a steady state (at $\sim 5 \times 10^{-12}$ s), most states are fairly tightly in equilibrium

with the 0^+ metastable state. This can be attributed to the large number of 1^- and 2^- states at energies greater than 4.4 MeV, which are accessible at this high temperature. As previously discussed, transition rates are very strong between levels of different parity that differ in spin by one or zero. Hence a large number of low-spin positive parity states can communicate with the 0^+ metastable state via the high-lying 1^- or 2^- states, which act as "pegs" anchoring the positive parity states to the metastable state. The exceptions are the high-spin 6^+ state at 3.51 MeV, which couples directly to the 5^+ ground state, and the 7^+ state at 3.92 MeV, which couples strongly to the aforementioned 6^+ state. Movies of the internal equilibration of ^{26}Al are available for viewing in the electron addendum to this paper [16].

VI. APPLICATION TO A NUCLEAR REACTION NETWORK

We now discuss how to use the effective transition rates between the ground and metastable states in a nuclear reaction network. The issue may be illustrated by computation of the effective ^{26}Al beta-decay lifetime in a stellar plasma. This discussion ultimately returns to the question mentioned in the introduction, namely, how to treat excited states in target nuclei, especially when the nucleus is not fully equilibrated internally.

In a stellar plasma, the ^{26}Al beta-decay rate is a linear combination of the beta-decay rates of the various excited states, weighted by their fractional population in an ensemble of ^{26}Al nuclei. When the temperature is high enough for the ^{26}Al nuclei to have equilibrated internally, the fractional populations of the excited states are given by the usual Boltzmann factors, and the effective beta-decay rate is relatively straightforward to compute. The difficulty arises when the nuclei do not rapidly equilibrate internally.

In calculations of the effective beta-decay rate, what one typically does is to follow internal transitions among many levels in the ^{26}Al nucleus with an implicit reaction network code. One also includes the beta-decay rates out of each level. Then, beginning with a particular abundance distribution among the nuclear levels, one evolves the network. The resulting effective beta-decay lifetime is then taken to be the time for the total ^{26}Al abundance to fall by a factor "e" [8,9].

While the above procedure certainly gives useful information, there is an ambiguity arising from the initial abundance populations if the transition rates between the ground and metastable states are small. For example, let us suppose the transition timescales between the two states are both shorter than 10^6 yr (the decay timescale of the ground state) but longer than 9.2 s (the decay timescale of the metastable state). If the nuclear reactions that produce ^{26}Al from other isotopes preferentially populate the ground state, the nuclei will (slowly) undergo a transition to the metastable state from which they will (rapidly) beta decay. The effective beta-decay lifetime will then essentially be the timescale to populate the metastable state. On the other hand, if the nuclear reactions preferentially populate the metastable state, the nuclei will largely beta decay before deexciting to the
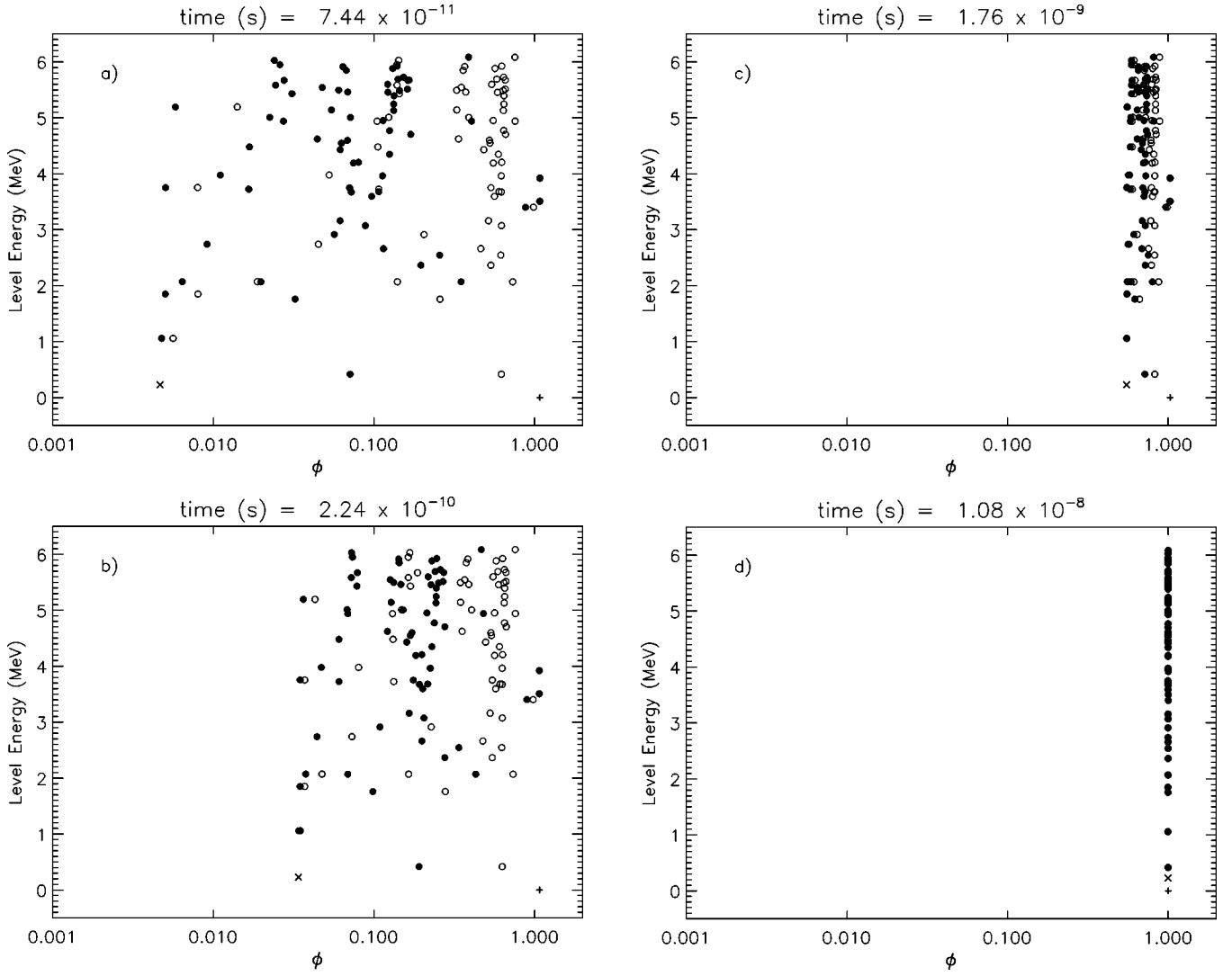
FIG. 8. The same as Fig. 7 except for $T_9 = 2.0$. A significant portion of the evolution in this case does not occur in a steady state. Indeed, for this temperature, the timescales to reach a steady state and equilibrium are nearly equal. The reason for this is that, for this temperature, the rates for upward transitions from levels 1 and 2 to the upper-lying levels are now comparable to the destruction rates of those upper-lying levels.

ground state. In this case, the effective beta-decay lifetime will be the beta-decay lifetime of the metastable state. There can be a large discrepancy in the effective beta-decay lifetimes in these two scenarios.

One could remove this ambiguity in a nuclear reaction network by including many levels in ^{26}Al as separate species. This becomes computationally burdensome. We seek here a means of treating the system as if it had only two nuclear species. To begin, we must be clear about those two species. From Eq. (5.9), the definition of the fugacity ϕ_k and the fact that $Y_k^{eq}/Y_q^{eq} = R_{qk}$, where R_{qk} is the "reverse ratio" previously defined as $(\lambda_{qk}/\lambda_{kq})$, we may find, under the assumption that the upper-lying levels are in a steady state, that

$$Y_k = \Gamma_{k1} R_{1k} Y_1 + \Gamma_{k2} R_{2k} Y_2 , \tag{6.1}$$

for levels $k > 2$. We define the weight factors at temperature T as

$$w_k^{(q)} = \begin{cases} \delta_{qk} & \text{if } k = 1,2, \\ \Gamma_{kq} R_{qk} & \text{if } k > 2 , \end{cases} \tag{6.2}$$

where $q = 1$ refers to the ground state and $q = 2$ to the metastable state, to permit use of the more compact equation

$$Y_k = w_k^{(1)} Y_1 + w_k^{(2)} Y_2 \tag{6.3}$$

for all levels k, $1 \leq k \leq n$. If we now take Y_{tot} to be the total number of ^{26}Al nuclei (at any excitation energy), we find

$$Y_{tot} = \left(\sum_k w_k^{(1)} \right) Y_1 + \left(\sum_k w_k^{(2)} \right) Y_2$$

$$= W_1 Y_1 + W_2 Y_2 \equiv Y_{(1)} + Y_{(2)} . \tag{6.4}$$

In this equation, $Y_{(1)}$ and $Y_{(2)}$ are the abundances of two ensembles of states. Ensemble (1) is comprised of the ground
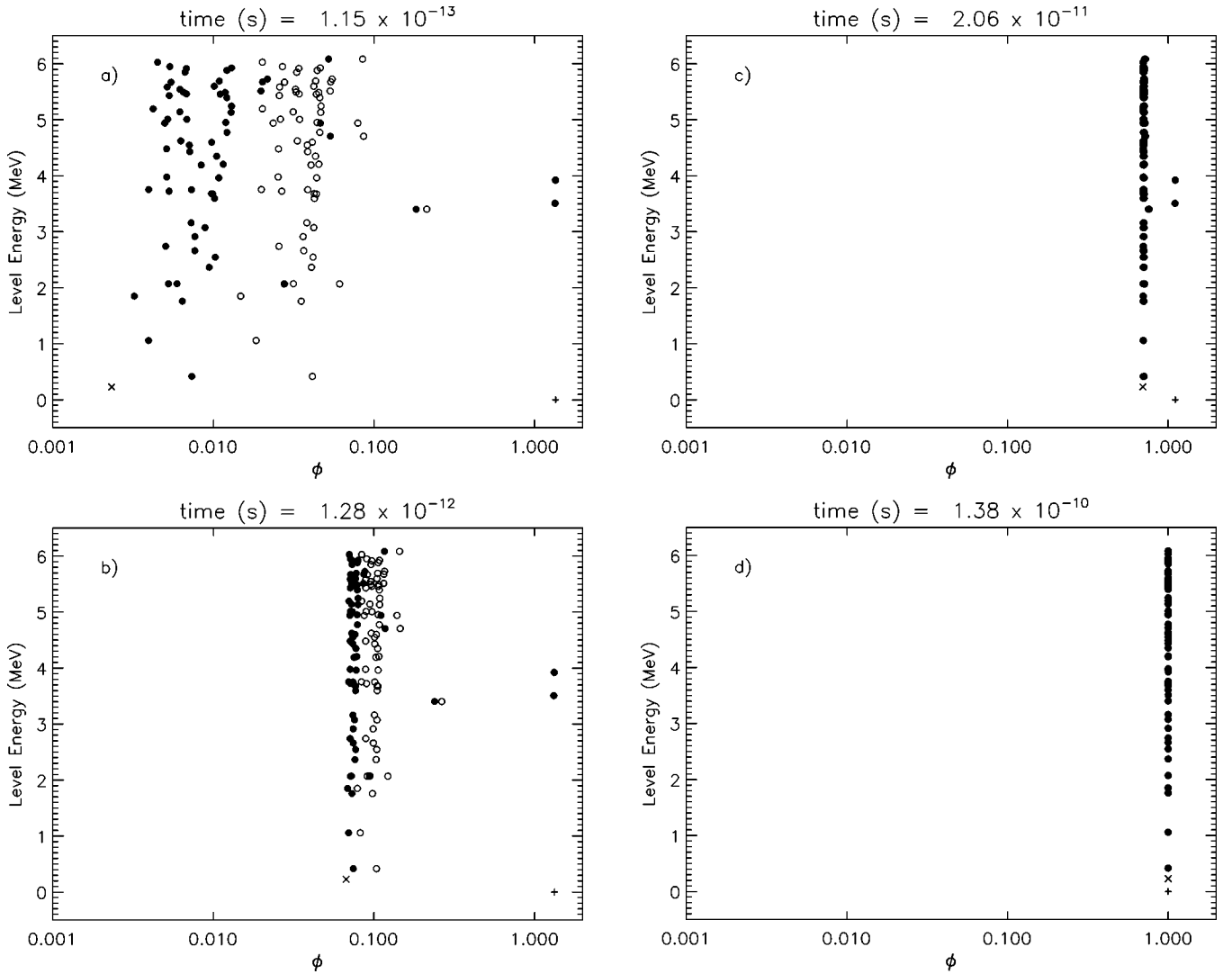
FIG. 9. The same as Fig. 7 except for $T_9 = 5.0$. A significant portion of the evolution in this case does not occur in a steady state. Surprisingly, however, more of the evolution is in a steady state than for $T_9 = 2.0$ (see Fig. 8). This is due to the accessibility of the high-lying 2^- states to which many lower-lying states are strongly connected. This greatly enhances the destruction rates of these levels so that they are faster than the upward transitions from levels 1 and 2. The accessibility of the high-lying 2^- states also provides a strong connection between most upper-lying levels to the 0^+ metastable state. This strongly enhances Γ_{k2} over Γ_{k1} for most upper-lying levels.

state and the portion of each upper-lying state connected to it via effective "cascades." Ensemble (2) is comprised of the metastable state and the portion of each upper-lying state connected to it via effective cascades. When treating the ^{26}Al nucleus as two separate species, it is in fact these two ensembles of states that are the two species, not the ground and metastable states [17]. The quantity $W_1(T)$ gives the enhancement of the abundance of ensemble (1) over the abundance of the ground state at temperature T. $W_1(T)$ will be nearly unity for low temperatures but will grow for higher temperatures as more of the ensemble (1) population resides in excited states. Similarly, $W_2(T)$ gives the enhancement of the abundance of ensemble (2) over the abundance of the metastable state at temperature T.

The crucial observation to be made here is that each of the two ensembles is in internal equilibrium, but the two ensembles are *not* in equilibrium with each other because the ground and metastable states are not in equilibrium. However, as the ground and metastable state abundances change, the abundances of any two levels within each ensemble change instantaneously to keep their ratio $(Y_j^{(q)}/Y_k^{(q)})$ $= (w_j^{(q)}/w_k^{(q)})$ a constant. Hence if we were following the evolution of one ensemble only, it would seem as if the abundances of levels in that ensemble were maintaining essentially unchanging "modified Boltzmann ratios" as constants of the evolution. What changes, at constant temperature, is the total number of nuclei in each of the two ensembles. Full internal equilibration occurs as these two numbers come into their correct equilibrium ratio. It is also essential to note that the ratio $w_j^{(q)}/w_k^{(q)}$ depends on the temperature; thus, the internal equilibria of the two ensembles will evolve in an environment with varying temperature.

It is now possible to compute the effective ^{26}Al beta-decay rate λ_β^{eff}. This rate is given by

$$\lambda_\beta^{eff} Y_{tot} = \sum_k \lambda_{\beta,k} Y_k, \qquad (6.5)$$

where $\lambda_{\beta,k}$ is the beta-decay rate out of nuclear level k. From Eq. (6.3), we may write

$$\lambda_\beta^{eff} Y_{tot} = \left(\sum_k \lambda_{\beta,k} w_k^{(1)} \right) Y_1 + \left(\sum_k \lambda_{\beta,k} w_k^{(2)} \right) Y_2$$

$$= \left(\frac{\sum_k \lambda_{\beta,k} w_k^{(1)}}{\sum_k w_k^{(1)}} \right) \left(\sum_k w_k^{(1)} \right) Y_1$$

$$+ \left(\frac{\sum_k \lambda_{\beta,k} w_k^{(2)}}{\sum_k w_k^{(2)}} \right) \left(\sum_k w_k^{(2)} \right) Y_2$$

$$= \left(\frac{\sum_k \lambda_{\beta,k} w_k^{(1)}}{\sum_k w_k^{(1)}} \right) W_1(T) Y_1$$

$$+ \left(\frac{\sum_k \lambda_{\beta,k} w_k^{(2)}}{\sum_k w_k^{(2)}} \right) W_2(T) Y_2$$

$$= \left(\frac{\sum_k \lambda_{\beta,k} w_k^{(1)}}{\sum_k w_k^{(1)}} \right) Y_{(1)} + \left(\frac{\sum_k \lambda_{\beta,k} w_k^{(2)}}{\sum_k w_k^{(2)}} \right) Y_{(2)}$$

$$\equiv \lambda_{\beta,1}^{eff} Y_{(1)} + \lambda_{\beta,2}^{eff} Y_{(2)}, \qquad (6.6)$$

where

$$\lambda_{\beta,q}^{eff} = \left(\frac{\sum_k \lambda_{\beta,k} w_k^{(q)}}{\sum_k w_k^{(q)}} \right) \qquad (6.7)$$

gives the effective beta-decay rate out of ensemble (q) and vindicates our choice of weight factor $w_k^{(q)}$ for level k in ensemble (q), as it leads to $\lambda_{\beta,q}^{eff}$ being the appropriately weighted ensemble average.

The weight factors provide more than conceptual insight into how each level influences the two ensembles; they also give us a compact vector formula for the effective beta-decay rate. We define the following vectors:
(i) The n-dimensional weight vectors

$$w_q = \begin{pmatrix} w_1^{(q)} \\ \vdots \\ w_n^{(q)} \end{pmatrix} \quad \text{for} \quad q = 1$$

(ground-state ensemble) and $q = 2$ (metastable-state ensemble);
(ii) The n-dimensional abundance vector

$$Y = \begin{pmatrix} Y_1 \\ Y_2 \\ Y_3^{SS} \\ \vdots \\ Y_n^{SS} \end{pmatrix};$$

and
(iii) The β-decay rate vector

$$\lambda_\beta = \begin{pmatrix} \lambda_{\beta,1} \\ \vdots \\ \lambda_{\beta,n} \end{pmatrix}.$$

With these definitions, Eq. (6.3) may be recast in matrix form as

$$Y = w_1 Y_1 + w_2 Y_2, \qquad (6.8)$$

and Eq. (6.7) as

$$\lambda_{\beta,q}^{eff} = \left[\frac{(\lambda_\beta)^T w_q}{W_q} \right]. \qquad (6.9)$$

Although our treatment has been of the effective beta-decay rate, the same formulas would apply for any reaction on ^{26}Al. For example, consider (p, γ) reactions on ^{26}Al. The proton capture rate

$$\lambda_{(p,\gamma)} = \begin{pmatrix} \lambda_{(p,\gamma),1} \\ \vdots \\ \lambda_{(p,\gamma),n} \end{pmatrix}$$

leads to

$$\lambda_{(p,\gamma),q}^{eff} = \left\{ \frac{(\lambda_{(p,\gamma)})^T w_q}{W_q} \right\}, \qquad (6.10)$$

where $\lambda_{(p,\gamma),k}$ is the rate of proton capture out of level k. All that is required to compute the (p, γ) reaction rates on ensembles (1) and (2) are (a) the $\lambda_{(p,\gamma),k}$ from experiment or calculation, (b) the known energies E_k, and (c) the weight factors $w_k^{(q)}$ ($q=1,2$) at a particular temperature, which we have calculated and tabulated along with the "cascade" probabilities Γ_{k1} and Γ_{k2} in the electronic addendum to this paper [16]. The reverse reactions, here the (γ,p) reactions, are derived from simple detailed balance. In full nuclear statistical equilibrium,

$$\lambda_{(\gamma,p),q}^{eff} \{ Y^{eq}(^{27}\text{Si}) \} = \lambda_{(p,\gamma),q}^{eff} \{ Y_{(q)}^{eq}(^{26}\text{Al}) \}. \qquad (6.11)$$

TABLE IV. Computed effective rates for the metastable- to ground-state transition and partition functions for the ensembles.

T_9	λ_{21}^{eff} (s^{-1})	$W_1(T)$	$W_2(T)$	$G_1(T)$	$G_2(T)$
0.0100	4.10300×10^{-96}	1.000000	1.000000	11.00000	1.000000
0.0125	4.15468×10^{-77}	1.000000	1.000000	11.00000	1.000000
0.0150	1.94459×10^{-64}	1.000000	1.000000	11.00000	1.000000
0.0175	2.18291×10^{-55}	1.000000	1.000000	11.00000	1.000000
0.0200	1.33873×10^{-48}	1.000000	1.000000	11.00000	1.000000
0.0250	4.26001×10^{-39}	1.000000	1.000000	11.00000	1.000000
0.0300	9.21628×10^{-33}	1.000000	1.000000	11.00000	1.000000
0.0400	7.64694×10^{-25}	1.000000	1.000000	11.00000	1.000000
0.0500	4.31367×10^{-20}	1.000000	1.000000	11.00000	1.000000
0.0600	6.34482×10^{-17}	1.000000	1.000000	11.00000	1.000000
0.0700	1.16137×10^{-14}	1.000000	1.000000	11.00000	1.000000
0.0800	5.77943×10^{-13}	1.000000	1.000000	11.00000	1.000000
0.0900	1.20700×10^{-11}	1.000000	1.000000	11.00000	1.000000
0.1000	1.37266×10^{-10}	1.000000	1.000000	11.00000	1.000000
0.1250	1.09171×10^{-8}	1.000000	1.000000	11.00000	1.000000
0.1500	2.01901×10^{-7}	1.000000	1.000000	11.00000	1.000000
0.1750	1.62241×10^{-6}	1.000000	1.000000	11.00000	1.000000
0.2000	7.74340×10^{-6}	1.000000	1.000000	11.00000	1.000000
0.2500	6.91072×10^{-5}	1.000000	1.000000	11.00000	1.000000
0.3000	3.22430×10^{-4}	1.000000	1.000000	11.00000	1.000000
0.4000	7.87669×10^{-2}	1.000000	1.000000	11.00004	1.000000
0.5000	9.47246×10^{0}	1.000040	1.000000	11.00044	1.000000
0.6000	2.34312×10^{2}	1.000200	1.000000	11.00221	1.000000
0.7000	2.32438×10^{3}	1.000630	1.000010	11.00698	1.000010
0.8000	1.31814×10^{4}	1.001500	1.000030	11.01655	1.000030
0.9000	5.35471×10^{4}	1.002950	1.000130	11.03241	1.000130
1.0000	1.86272×10^{5}	1.005040	1.000430	11.05547	1.000430
1.2500	3.75137×10^{6}	1.013220	1.005950	11.14545	1.005950
1.5000	4.79670×10^{7}	1.024410	1.062240	11.26849	1.062240
1.7500	2.97220×10^{8}	1.033290	1.353300	11.36617	1.353300
2.0000	9.44006×10^{8}	1.032540	2.023560	11.35792	2.023560
2.5000	3.26551×10^{9}	1.019130	3.383490	11.21046	3.383490
3.0000	8.91509×10^{9}	1.012520	4.200290	11.13769	4.200290
4.0000	6.03840×10^{10}	1.007600	5.364650	11.08361	5.364650
5.0000	2.99268×10^{11}	1.008740	6.408690	11.09616	6.408690
6.0000	1.09493×10^{12}	1.017320	7.504550	11.19057	7.504550
7.0000	3.06342×10^{12}	1.037320	8.689610	11.41049	8.689610
8.0000	6.89206×10^{12}	1.071750	9.978150	11.78920	9.978150
9.0000	1.31576×10^{13}	1.120540	11.40326	12.32598	11.40326
10.0000	2.22906×10^{13}	1.181160	13.00940	12.99279	13.00940

This leads to

$$\lambda_{(\gamma,p),q}^{eff} = \lambda_{(p,\gamma),q}^{eff} W_q \left\{ \frac{Y_q^{eq}(^{26}\text{Al})}{Y^{eq}(^{27}\text{Si})} \right\}. \qquad (6.12)$$

In this way, the usual detailed balance result for deriving the reverse reactions applies. The crucial points are (a) that the two ^{26}Al species must have the masses of the ^{26}Al ground ($q=1$) and metastable ($q=2$) states and (b) that the partition functions for the two species are $G_{(1)}(T) = (2J_1 + 1)W_1(T) = 11W_1(T)$ and $G_{(2)}(T) = (2J_2 + 1)W_2(T)$ $= W_2(T)$. From these results, all proper relations among reactions will follow. Given the validity of the (largely appropriate) assumption of a steady state among the upper-lying levels, this treatment allows for a simple and accurate treatment of the effect of excited states on target nuclei when an inefficient communication between the ground state and the first excited state inhibits internal equilibration of the nucleus.

We must finally turn to the question of the interaction of the two ensembles because now we are properly evolving them, rather than the abundances of the ground and metastable states. If we consider only changes due to internal
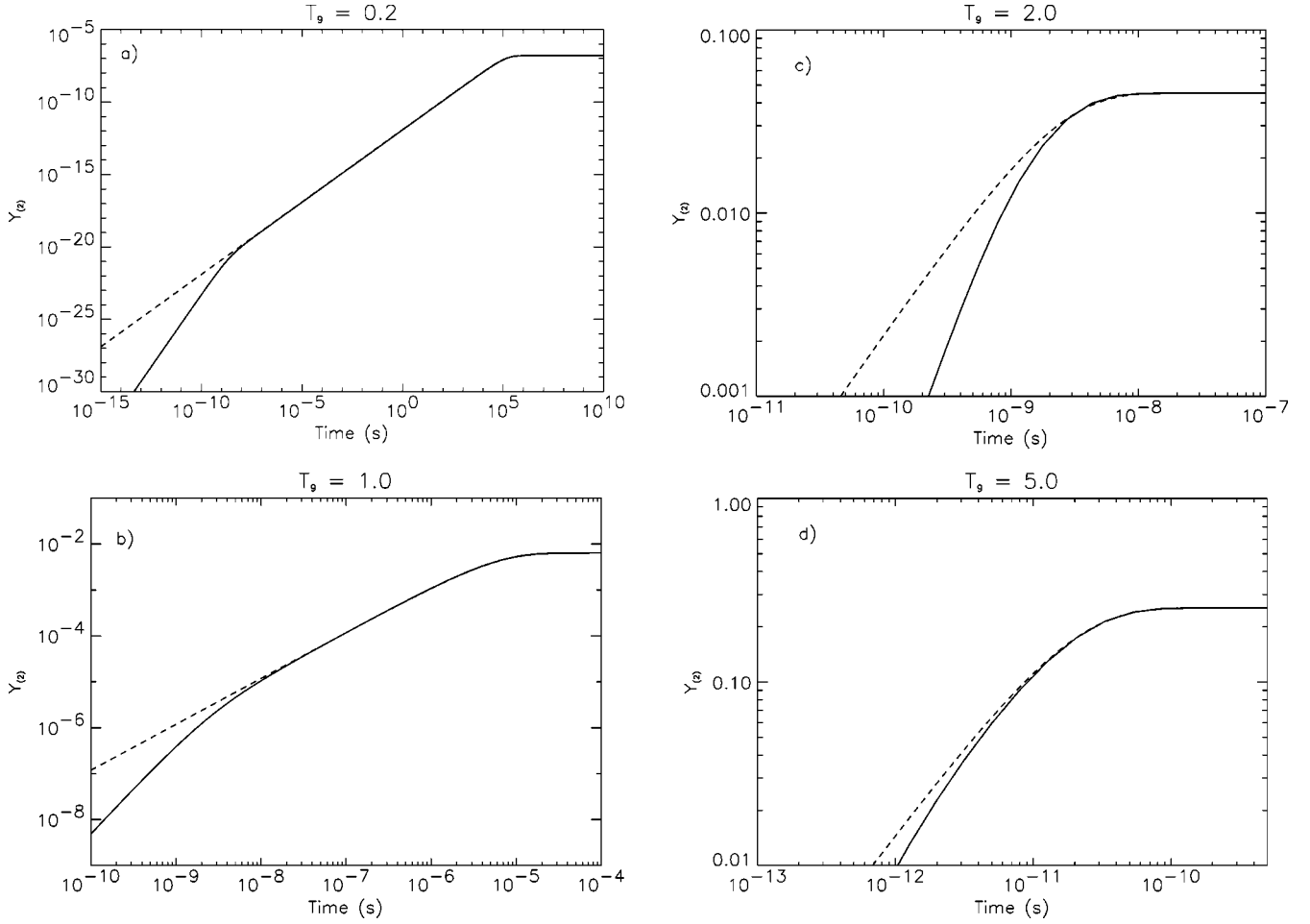
FIG. 10. Evolution of the abundance of ensemble (2) of states in ^{26}Al as a function of time for $T_9 = 0.2$, 1.0, 2.0, and 5.0. In each panel, the solid curve gives the ensemble abundance derived from the results in the full network calculation while the dashed curve gives the result when the ensembles are evolved using the effective rates $\lambda^{eff}_{(12)} = (\lambda^{eff}_{12}/W_1)$ and $\lambda^{eff}_{(21)} = (\lambda^{eff}_{21}/W_2)$. Below a temperature $T_9 \lesssim 2.0$, using a two-state system with effective transition rates gives a perfectly accurate representation of the full network. At higher temperatures, however, the steady-state approximation we employ to compute the effective rates overestimates the abundances of the upper-lying levels. This causes the effective two-state system to evolve more rapidly than in the actual network. Nevertheless, even for such cases, the internal equilibration timescale is well reproduced, and the treatment of the levels in the ^{26}Al nucleus as two ensembles of states is well justified at all temperatures.

transitions, then

$$\frac{dY_{tot}}{dt} = \left[\frac{dY_1}{dt} + \frac{dY_2}{dt}\right] + \sum_{k>2}\left(\frac{dY_k}{dt}\right) = 0, \qquad (6.13)$$

because the total number of nuclei remains fixed. The last term in Eq. (6.13) is zero under our assumption of a steady state; therefore,

$$\frac{dY_{tot}}{dt} = \left(\frac{dY_1}{dt} + \frac{dY_2}{dt}\right)$$

$$= -\lambda^{eff}_{12}Y_1 + \lambda^{eff}_{21}Y_2 + \lambda^{eff}_{12}Y_1 - \lambda^{eff}_{21}Y_2$$

$$= -\left\{\frac{\lambda^{eff}_{12}}{W_1}\right\}Y_{(1)} + \left\{\frac{\lambda^{eff}_{21}}{W_2}\right\}Y_{(2)}$$

$$+ \left\{\frac{\lambda^{eff}_{12}}{W_1}\right\}Y_{(1)} - \left\{\frac{\lambda^{eff}_{21}}{W_2}\right\}Y_{(2)}$$

$$\equiv -\lambda^{eff}_{(12)}Y_{(1)} + \lambda^{eff}_{(21)}Y_{(2)} + \lambda^{eff}_{(12)}Y_{(1)} - \lambda^{eff}_{(21)}Y_{(2)},$$
$$(6.14)$$

where we have used Eq. (6.4) to replace the abundances of the ground and metastable states with the populations of the two ensembles. Because $dY_{tot}/dt = dY_{(1)}/dt + dY_{(2)}/dt$, we can infer from Eq. (6.14) that

$$\frac{dY_{(1)}}{dt} = -\left\{\frac{\lambda^{eff}_{12}}{W_1}\right\}Y_{(1)} + \left\{\frac{\lambda^{eff}_{21}}{W_2}\right\}Y_{(2)} = -\lambda^{eff}_{(12)}Y_{(1)} + \lambda^{eff}_{(21)}Y_{(2)}$$
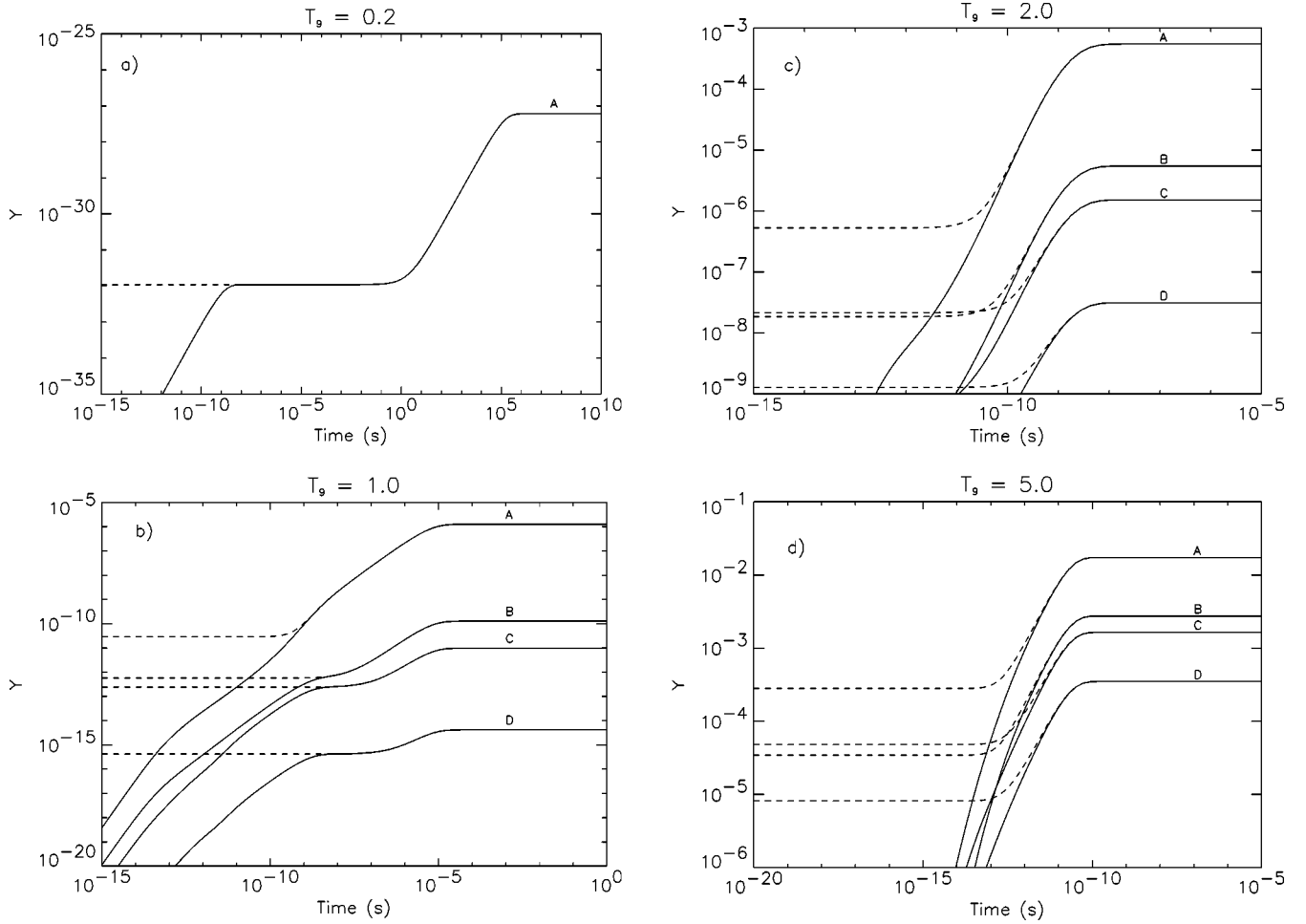$$(6.15)$$

and

FIG. 11. Evolution of the abundances of levels 4 at 1058 keV (A), 6 at 1851 keV (B), 9 at 2072 keV (C), and 13 at 2740 keV (D) in ^{26}Al at $T_9 = 0.2$, 1.0, 2.0, and 5.0. The solid curve gives the actual network abundances while the dashed curve gives the steady-state abundances. At low temperature, much of the evolution of network abundances occurs in a steady state; therefore, the approximation used in our calculation of the effective rate is excellent. At higher temperatures, the upper-lying levels achieve a steady state only shortly before they reach their equilibrium values. This means that throughout much of the evolution, the steady-state approximation overestimates the abundances of the upper-lying levels with the consequence that the effective transition rates from ensemble (1) to (2) and vice versa are likewise overestimated for a large part of the evolution.

$$\frac{dY_{(2)}}{dt} = \left\{ \frac{\lambda_{12}^{eff}}{W_1} \right\} Y_{(1)} - \left\{ \frac{\lambda_{21}^{eff}}{W_2} \right\} Y_{(2)} = \lambda_{(12)}^{eff} Y_{(1)} - \lambda_{(21)}^{eff} Y_{(2)} .$$

(6.16)

These equations are the modified form of Eq. (2.15) that properly account for the abundances of the ensembles rather than those of levels 1 and 2. In equilibrium, both $dY_{(1)}/dt \rightarrow 0$ and $dY_{(2)}/dt \rightarrow 0$, thereby giving

$$\frac{Y_{(2)}^{eq}}{Y_{(1)}^{eq}} = \frac{W_2(T)}{W_1(T)} \frac{\lambda_{12}^{eff}}{\lambda_{21}^{eff}} = \frac{W_2(T)}{W_1(T)} \frac{Y_2^{eq}}{Y_1^{eq}} = \frac{G_{(2)}(T)}{G_{(1)}(T)} e^{-E_2/kT} .$$

(6.17)

The ratio of the equilibrium abundances of ensembles (1) and (2) is therefore the ratio of the equilibrium abundances of the ground and metastable states, respectively, corrected for the relative enhancements of the two ensembles. The values of $W_1(T)$, $W_2(T)$, and the partition functions of the two ensembles $G_1(T)$, $G_2(T)$ at different temperatures T are

tabulated in Table IV along with the effective rates between the ground and metastable states. We also present on the web a FORTRAN subroutine that computes λ_{21}^{eff}, λ_{12}^{eff}, W_1, and W_2 (see the electronic addendum [16]). This subroutine renders the calculation of ensemble (1) and (2) populations straightforward at any temperature.

Figure 10 shows that the evolution of the ensemble (2) population using effective rates (dashed line) gives the correct equilibration timescale when compared to the ensemble population in the full network calculation (solid line). Though the evolution using effective rates begins to diverge from that in a full network calculation at $T_9 \approx 1.0$, the time taken to reach equilibrium is still correct even at $T_9 = 5.0$. In making this comparison we have used $Y_{(2)} = W_2(T)Y_2$ for the ensemble (2) population resulting from the steady-state assumption and

$$Y_{(2)}^{net} = Y_2 + \sum_{k>2} \left\{ \left(\frac{w_k^{(2)} Y_2}{w_k^{(1)} Y_1 + w_k^{(2)} Y_2} \right) Y_k \right\}$$

(6.18)

for the ensemble population in the full network calculation. Here Y_2 and Y_k refer to level abundances as returned by the full network and the definition of $Y_{(2)}^{net}$ apportions the actual network abundance of the upper-lying levels into a part belonging to ensemble (2). This seems to be the fairest way of computing the abundance of ensemble (2) when the upper-lying levels are not necessarily in a steady state. Keeping in mind that both axes in the plot are logarithmic, we can see that $Y_{(2)}^{SS}$ and $Y_{(2)}^{net}$ actually coincide for a significant part of the evolution even at high temperatures.

An important observation that results from Fig. 10 is that the effective rate is actually *faster* than the rate for the full network. One might think that a truncation of the matrix series would underestimate the effective rate, but that is not the case. To explain this behavior, we must investigate not only the time evolution of the ground and the metastable states, but also of the upper-lying levels. We may find the steady-state abundance of an upper-lying level from Eq. (3.22). In Fig. 11 we compare the steady-state abundances (dashed lines) of levels 4, 6, 9, and 13, which are all 1^+ states located at 1057.74 keV, 1850.62 keV, 2071.64 keV, and 2740.03 keV, respectively, to their actual network evolution (solid lines) at different temperatures. We notice that at low temperatures the levels attain steady states rather quickly, and hence the steady-state assumption that assigns them the Y_k^{SS} from the beginning is a good one. However, at higher temperatures the steady-state approximation overestimates the population of the upper-lying levels for a significant fraction of the total time required to reach equilibrium. Since the approximation overestimates the production of the higher-lying intermediate levels, it automatically overestimates the effective rate to go from the metastable to the ground state via transitions involving those higher levels. However, as Fig. 10 amply demonstrates, the only effect is on *how* equilibrium is reached: the time taken to reach it is unaffected.

The equations derived in this section allow for a complete reduction of an ^{26}Al system to two separate species (two ensembles of states). This treatment is perfectly accurate if the assumption of a steady state among the upper-lying levels holds. This will always be the case as long as the time scales for deexcitation of the upper-lying levels dominate the timescales for destruction of those levels by light particle capture or weak decay or the timescales for production from the ground or metastable state.

VII. SUMMARY

We have computed the effective rate of internal equilibration of a nucleus with a long-lived isomeric state. The underlying assumption of our work is that the upper-lying levels in the nucleus attain a steady state much faster than do the ground or metastable state. At low temperatures, this is a perfectly valid approximation, and the resulting effective rate generally provides an excellent description of the equilibration of the nucleus.

We have also computed the degree of connection of any upper-lying level (in a steady state) to the ground or metastable state. This allowed us to separate the nuclear levels of an isotope with a long-lived metastable state into two ensembles of states. We then showed how to compute rates for transition into, out of, and between these two ensembles. These ensembles, then, are the proper ''species'' to evolve in the nuclear reaction network, and we have completely reduced the nuclide to a two-state system. We have illustrated our technique with the specific example of the interesting isotope ^{26}Al, but we will consider other important isotopes in future work.

[1] T. A. Weaver and S. E. Woosley, Phys. Rep. **227**, 65 (1993).

[2] R. Bonetti *et al.*, Phys. Rev. Lett. **82**, 5205 (1999).

[3] N. A. Bahcall and W. A. Fowler, Astrophys. J. **157**, 659 (1969); **157**, 645 (1969).

[4] C. Angulo *et al.*, Nucl. Phys. **A656**, 3 (1999); T. Rauscher and F.-K. Thielemann, At. Data Nucl. Data Tables **75**, 1 (2000).

[5] J. Knödlseder *et al.*, Astron. Astrophys. **345**, 813 (1999).

[6] R. H. Nichols, F. A. Podosek, B. S. Meyer, and C. L. Jennings, Meteorit. Planet. Sci. **34**, 869 (1999).

[7] C. Travaglio *et al.*, Astrophys. J. **510**, 325 (1999).

[8] R. A. Ward and W. A. Fowler, Astrophys. J. **238**, 266 (1980).

[9] A. Coc, M.-G. Porquet, and F. Nowacki, Phys. Rev. C **61**, 015801 (2000).

[10] H. Minc, *Nonnegative Matrices* (Wiley, New York, 1988).

[11] N. Pullman, *Matrix Theory and Its Applications: Selected Topics* (Marcel Dekker, New York, 1976).

[12] B. N. Datta, *Numerical Linear Algebra* (Brooks-Cole, Pacific Grove, Ca, 1995).

[13] R. P. Stanley, *Enumerative Combinatorics* (Cambridge University Press, Cambridge, 1997).

[14] A. V. Aho, J. E. Hopcroft, and J. Ullman, *Data Structures and Algorithms* (Addison-Wesley, Reading, MA, 1983).

[15] R. C. Runkle, A. E. Champagne, and J. Engel, Astrophys. J. (to be published).

[16] See EPAPS Document No. E-PRVCAN-64-028108 for the electronic addendum to this paper. It includes figures, tables, and movies. EPAPS document files may be retrieved free of charge from our FTP server (http://www.aip.org/pubservs/epaps.html) or from ftp.aip.org in the directory /epaps/. See the EPAPS homepage for more information.

[17] G. M. Fuller, W. A. Fowler, and M. J. Newman, Astrophys. J., Suppl. **42**, 447 (1980).